

Allogenic controls on organic matter accumulation in the Woodford Shale in southern Oklahoma

by

Brayton Avery Pew

B.S., Purdue University, 2019

A THESIS

submitted in partial fulfillment of the requirements for the degree

MASTER OF SCIENCE

Department of Geology
College of Arts and Sciences

KANSAS STATE UNIVERSITY
Manhattan, Kansas

2021

Approved by:
Major Professor
Karin Goldberg

Copyright

© Brayton Pew 2021.

Abstract

The Woodford Shale is an organic-rich formation found in southern Oklahoma and Kansas and has been extensively studied due to recent advancements in hydrocarbon recovery in mudrock successions. The controls on organic matter formation and preservation within the Woodford are not entirely clear in southern Oklahoma, but previous work points towards upwelling and anoxic bottom-waters as leading factors for the high organic content. This study was performed on a Woodford Shale outcrop located along Interstate 35 (mile marker 44) in Carter County, Oklahoma and contains the middle and upper Woodford succession. The integration of facies and chemical analyses, including hand-held X-ray fluorescence (HHXRF), inductively-coupled plasma mass spectrometry (ICP-MS), X-ray diffraction (XRD) and total organic carbon (TOC), were performed to construct sedimentologic-chemostratigraphic logs that allowed the establishment of a stratigraphic framework and evaluation of depositional parameters such as detrital input, primary productivity, and degree of oxygenation during the accumulation of the studied succession. The I-35 Woodford Shale outcrop can be divided into three main sequences (1, 2, and 3, from base to top), with sequences 2 and 3 further subdivided into subsequences (A and B), based on changes in chemostratigraphic indices proxies for detrital input, primary productivity, and degree of oxygenation, and accompanied facies associations. Sequence 1 is characterized by distal, pelagic settling sediments with 12-13% TOC deposited under conditions of stable anoxia/euxinia, with low-moderate primary productivity. Sequence 2A is defined by interbedded pelagic and hemipelagic deposits with TOC between 7-11%. It was deposited in more oxic environments because of decreased water depths, resulting in less preservation of organics. The continued accumulation of pelagic and hemipelagic deposits in Sequence 2B is accompanied by increased primary productivity following an increase in nutrient

supply from upwelling and continental waters, which resulted in organic contents of about 12%. The hemipelagic deposits of Sequence 3A display the highest TOC in the entire succession (14-20%), as a consequence of productivity boosts due to riverine nutrient input, despite the presence of overall oxic bottom waters with occasional anoxic events. Sequence 3B accumulated in a low to moderately productive environment under strongly anoxic conditions, resulting in the lowest TOC in the entire section (2-8%). The detailed study of the I-35 Woodford Shale outcrop indicates that high organic content (TOC>10%) is found in settings where primary productivity is high, regardless of the bottom-water conditions. Primary productivity was boosted by riverine nutrient input associated with shallowing waters. The results of this study suggest that organic flux is more important than anoxia in the burial of organics in the sediments, with anoxia oftentimes being a consequence of high organic flux.

Table of Contents

List of Figures	vi
List of Tables	vii
Acknowledgements	viii
Dedication	ix
Chapter 1 - Introduction	1
Chapter 2 - Geologic Background	3
Chapter 3 - Methods	6
Chapter 4 - Results	17
Chapter 5 - Discussion	23
Chapter 6 - Conclusions	28
References	29
Appendix A - HHXRF Data	33
Appendix B - XRD Diffractograms	59

List of Figures

Figure 1: Images from Google Earth showing the study outcrop on I-35 (red dot), located in the Arbuckle Mountains (southern anticline).	2
Figure 2: Paleogeographic reconstruction of North America in the Late Devonian (360 Ma). Red circle represents the study area (Map from Blakey, 2013).	5
Figure 3: Template from Lazar et al. (2015) used for construction of the sedimentary log.	7
Figure 4: : Sedimentologic and chemostratigraphic log from the I-35 outcrop, with interpretations of depositional environment and stratigraphic framework.	8
Figure 5: Diffractogram (bulk analysis) for sample OK-1-1. Major peaks match with those of quartz, biotite, and magnesioferrite.....	21
Figure 6: ICP-MS vs HHXRF concentration of Mo (in ppm)	22
Figure 7: Photomicrograph of radiolarians (white circles) and pyrite (black clusters) found in samples from Sequence 1.....	27
Figure 8: Photomicrograph of Tasmanites (thin orange bioclasts) immersed in clay matrix with scattered fine quartz grains (Sequence 1).	27

List of Tables

Table 1: Facies identified for the I-35 outcrop section	10
Table 2: Carbonate, Total Organic Carbon (TOC), and Sulfur weight % for samples from I-35 outcrop.	14
Table 3: ICP-MS data for samples from the I-35 outcrop.	15

Acknowledgements

I would like to thank my advisor, Dr. Karin Goldberg, for her support and guidance throughout this project. This project would not have been possible without her and I could not have asked for a better mentor through this journey. I would also like to thank my committee members, Drs. Matthew Brueseke and Matthew Kirk, for their feedback and support. I would also like to thank Dr. Brice LaCroix and Hallie Bruce for all their help with XRD analysis and preparation, Dr. Pamela Kempton for her help with the hand-held X-ray Fluorescence, and Jade Mountain for helping in the preparation of samples used in this project. Finally, I would like to say thank you to my parents, Troy and Stacey, and my siblings, extended family, and friends for their continued support of this long journey I have been on for the past six years.

Dedication

I would like to dedicate this work to my grandfather, Jack. His interest in the natural world and what it has to offer has guided me to this point.

Chapter 1 - Introduction

The Woodford Shale is a well-studied formation due to its high organic matter concentration, which, coupled with furthered advancements in hydrocarbon recovery in mudrocks, allowed for the exploitation of this unit. The primary driving mechanisms for organic accumulation in the Woodford of southern Oklahoma are not entirely clear, but possible drivers such as anoxic bottom waters and increased productivity have been studied extensively by several authors (e.g. Slatt et al. 2012; Turner et al. 2016). In general, high organic content in mudrocks have been attributed to either, or a combination, of these parameters (Goldberg and Humayun, 2016).

The aim of this study is to integrate sedimentologic and chemostratigraphic analyses to identify the specific environmental conditions (e.g., degree of oxygenation, primary productivity, rate of sediment supply) and overall controls on sedimentation of the Woodford Shale in southern Oklahoma while defining the main switches in organic matter accumulation.

This study was carried out on a Woodford Shale outcrop along Interstate 35 (mile marker 44) in Carter County, Oklahoma (Fig.1), where a detailed, mm-cm facies description was made, and 240 samples were collected for petrographic and chemical analyses. The integration of these analyses aimed to help constrain the environmental and paleogeographic settings that led to the development of organic-rich horizons found in the Woodford. Understanding the controls on organic matter accumulation in the Woodford helps the identification of potential future unconventional source rocks deposited under similar settings and conditions.



Figure 1: Images from Google Earth showing the study outcrop on I-35 (red dot), located in the Arbuckle Mountains (southern anticline).

Chapter 2 - Geologic Background

The Woodford Shale was deposited during the late Devonian and early Mississippian across Kansas and Oklahoma and is laterally equivalent to the Chattanooga, Ohio, New Albany, and Barnett shales found in the eastern and southeastern parts of the Appalachian Basin. During the deposition of the Woodford, North America was part of a large landmass south of the equator (Fig. 2) (Blakey, 2013). Works by Schieber (1998), Hemmesch et al. (2014), and Li and Schieber (2015) suggest that Woodford Shale and its lateral equivalents were deposited in a shallow inland sea, based on observed shallow-water sedimentary structures (cross-stratification, phosphate accumulation, erosional surfaces, and storm deposits) with bottom-water conditions alternating between suboxic and dysoxic. The I-35 Woodford outcrop was likely deposited under a mostly transgressive sequence during the formation of its lower and middle sections, and a regressive sequence during the deposition of the upper part of the section (Turner et al., 2016).

Organic-rich zones within the Woodford could be controlled by upwelling or riverine nutrient input, but there is a consensus that the organic zones are due to upwelling (Comer, 2008). Upwelling can occur in both coastal and equatorial settings, so paleogeographic reconstructions are an essential factor when determining upwelling type in the Woodford Shale. Reconstructions from Blakey (2013) places southern Oklahoma near the equator in a shallow marine setting at 360 Mya (Fig. 2), indicating that equatorial upwelling would be the main upwelling type. Previous works have concluded that this part of southern Oklahoma would have been subject to equatorial winds that could have driven upwelling (Parrish and Curtis, 1982).

Other evidence in marine stratigraphic successions that is indicative of paleo-upwelling is the presence of bedded cherts, phosphate nodules, and organic-rich rocks (Kidder and Erwin, 2001), all of which are found in the Woodford Shale. Bedded cherts form in zones of increased productivity due to

accumulation of radiolarians and siliceous sponges (Kidder and Erwin, 2001). However, an increase in silica-rich beds could also be attributed to the increase of silica from riverine input and erosion from recent orogenic events (Kidder and Erwin, 2001).

Slatt et al. (2012) have identified at least eight different lithofacies throughout the lower, middle, and upper Woodford in Pontotoc County, Oklahoma, using similar methods used in this study (see below in Chapter 3 - Methods). Facies similar to those identified by Slatt et al. (2012) in their study of the Lower-Middle-Upper sections of the Woodford were recognized in this study. Namely, their black laminated shale is the ShO in this study, their silica laminated shale, the ShR, and their nodular laminated shale was described in this study as silica nodules in the ShR and ShO facies (Chapter 4).

Several theses have investigated other aspects of the Woodford Shale, such as the effect of organic matter on illitization (Janssen, 2017) and the control of mineralogy in brittleness (Wehner, 2018). Brower (2019) used the same methodology as this study to analyze a drill core of the Chattanooga Formation (Woodford Shale equivalent) in Kansas. His findings suggested that the main control on organic accumulation in sediments was primary productivity. Furthermore, he suggested that anoxic bottom waters were driven by increased primary productivity which led to the formation of organic-rich sediments.

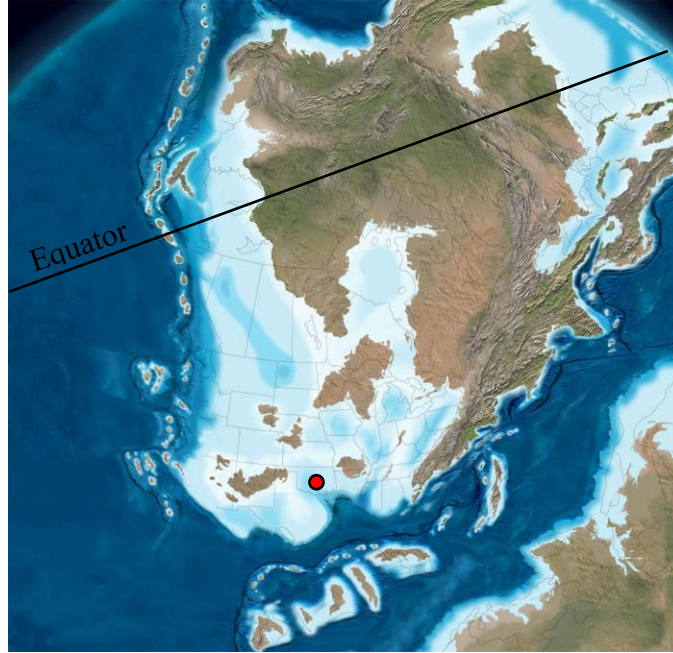


Figure 2: Paleogeographic reconstruction of North America in the Late Devonian (360 Ma). Red circle represents the study area (Map from Blakey, 2013).

Chapter 3 - Methods

Facies analysis

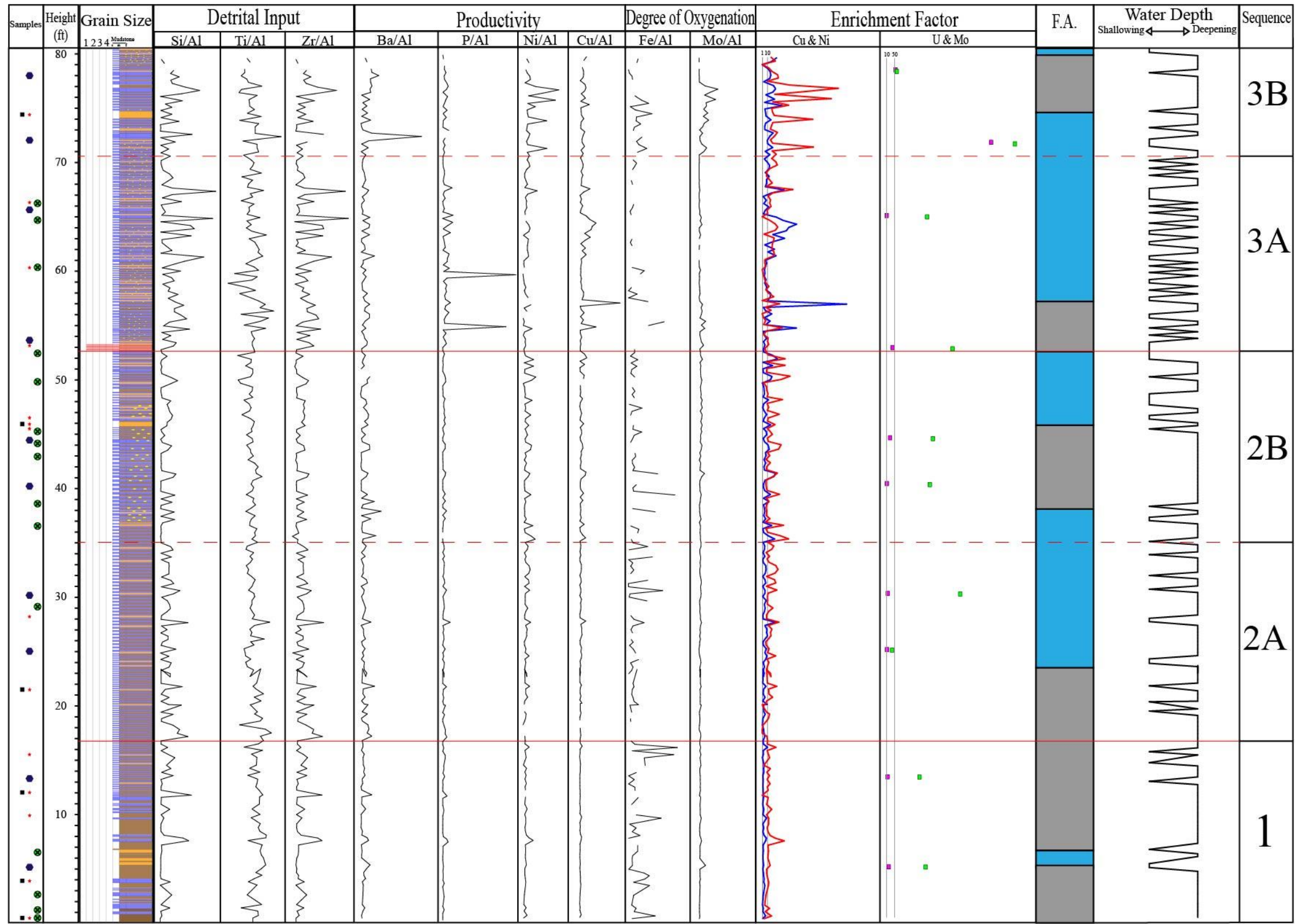
A detailed lithofacies description was performed on the I-35 outcrop (mile marker 44) in Carter County, Oklahoma using a stratigraphic template from Lazar et al. (2015) (Fig. 3). The I-35 outcrop was chosen due to ease of access to the entirety of the middle and upper sections of the Woodford. The description included grain size, lithology, estimated organic concentration, color, sedimentary structures, presence of nodules and fracture patterns. Descriptions were summarized in a chemostratigraphic sedimentary log (Fig. 4) and organized in a facies table. The chemostratigraphic log was constructed with grain size on the x-axis, bedding thickness on the y-axis, and paired with sedimentary structures, facies names, facies descriptions, photographs and collected samples, and calculated chemical indices for detrital input (Tribovillard et al. 2006), primary productivity (Tribovillard et al. 2006), and degree of oxygenation (Algeo and Maynard, 2008; Arnaboldi and Meyers, 2007; Tribovillard et al. 2006), and made into a digitalized version with Adobe Illustrator. Facies codes consist of letters that represent the lithology of the samples (e.g. Sh for shale, R for radiolarites) accompanied by other major features (e.g., O for organic). The facies were then grouped into facies associations, a group of facies genetically related to each other, and which represent environments of deposition within a depositional system (James and Dalrymple, 2010; Collinson, 1996).

Samples for petrographic and geochemical analyses were collected every 10 cm, totaling 240 samples for the entire section. Samples were obtained using a rock hammer and chisel, starting at the base of the outcrop up to where vegetation prevented further collection.

Well/Chokeover: _____ Location: _____ Page: _____ of _____

Depth (#)	Lithology, texture, Bed surface				Composition		Soil Strat. Horizons				Topography		Notes Bedrock, fossils, etc., stratigraphy, paleontology, etc. (Mudstone, siltstone, sandstone, etc., etc.)	EOD
	Clay Sh Silt St	Silt Sh Clay St	MS MS MS MS											

Figure 3: Template from Lazar et al. (2015) used for construction of the sedimentary log.



Ranges of Indices

Si/Al Max: 258.43 Min: 4.52	Mo/Al Max: 0.07 Min: 7.3e-6	Ni/Al Max: 0.04 Min: 0.0004
Ti/Al Max: 0.11 Min: 0.02	Ba/Al Max: 1.10 Min: 0.001	P/Al Max: 1.60 Min: 0.004
Zr/Al Max: 0.31 Min: 0.0005	Fe/Al Max: 3.44 Min: 0.006	Cu/Al Max: 0.05 Min: 2.9e-8

Legend

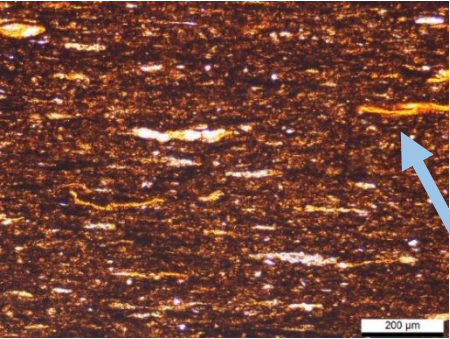
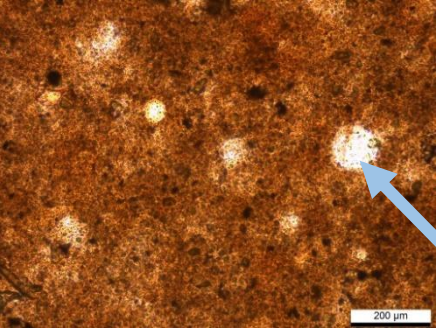
Organic-rich Shale (ShO)	Grain Size
Siliceous Shale (ShR)	1 = Cgl
Radiolarite (R)	2 = Coarse Sandstone
Intraformational Conglomerate (CI)	3 = Medium Sandstone
Nodule (S=Silica and P=Phosphate)	4 = Fine Sandstone
Thin Section	Mudstone
LECO and ICP-MS	C Coarse
XRD	M Medium
Photograph	F Fine
	EF Cu
	EF Ni
	EF U
	EF Mo
	Hemipelagic Settling
	Pelagic Settling

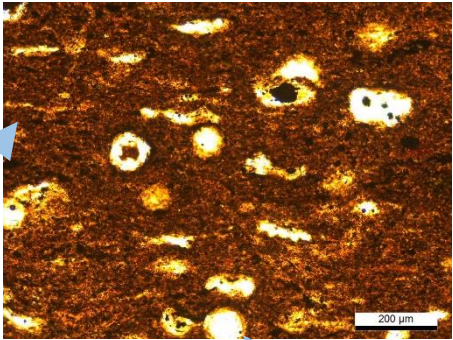
Figure 4: Sedimentologic and chemostratigraphic log from the I-35 outcrop, with interpretations of depositional environment and stratigraphic framework.

Petrographic analysis

From the 240 samples collected, 14 were made into thin sections. These 14 samples were chosen either to represent the different lithofacies identified in the field, or to check specific characteristics (e.g., amount and type of organics, unique color, or determine unknown lithology based on field observations). Qualitative petrographic analysis was carried out to augment lithofacies descriptions and detect subtle changes (in grain size and/or composition) that would aid interpretation of features observed in the field, or even detect new lithofacies, if any were missed. The results of this analysis are not reported for individual thin sections but included in the summary of the lithofacies in Table 1.

Table 1: Facies identified for the I-35 outcrop section

Facies Code	Description	Interpretation	Outcrop Photo	Photomicrograph
ShO	Organic-rich clayey shale, brownish-black (5YR 4/1), laminated, with fine fissility. In thin section, abundant Tasmanites and amorphous organic matter (AOM), rare phytoclasts and agglutinated foraminifers. Radiolarians less than 10%, if present. Rare scattered silt grains.	Pelagic settling (Stow et al. 2001; Stow and Smillie, 2020) under high primary marine organic productivity (Peng 2021), with contribution from algal blooms (Loucks and Ruppel 2007)		<p data-bbox="2149 315 2355 347">Plane polarizers</p>  <p data-bbox="2507 656 2662 737">Agglutinated foraminifer</p>
R	Radiolarite, dark black (5 YR 2/1) with conchoidal and vertical fractures, very hard, massive or laminated. In thin section, radiolarians comprise more than 50%, embedded in clay matrix	Pelagic settling (Stow and Smillie, 2020), with contribution from blooms of radiolarians (Loucks and Ruppel 2007).		 <p data-bbox="2507 1276 2662 1308">Radiolarian</p>

<p>ShR</p>	<p>Siliceous clayey shale, with medium-coarse fissility, laminated. In thin section, radiolarians comprise between 10-50%, with subordinate Tasmanites and AOM. Rare mm silt laminae.</p>	<p>Alternating deposits of low-density turbidity currents and pelagic fallout (Peng 2021; Talling et al., 2012).</p>		 <p>Tasmanites</p> <p>Radiolarian</p>
<p>CI</p>	<p>Intraformational conglomerate, light gray (M-6), composed of angular, irregular clasts, of radiolarite and siliceous shale (R and ShR) in a medium-coarse sand matrix.</p>	<p>Rip-up clasts eroded from water-rich, partially consolidated mud at the sea floor, transported as bedload and deposited when the flow decelerates (Peng 2021)</p>		<p>See R and ShR photomicrographs</p>

Hand-held X-ray fluorescence

Hand-held X-ray fluorescence (HHXRF) has become a powerful method for finding heterogeneity within a homogeneous appearing mudrock (Turner et al., 2016). For this study, elemental concentrations for major and trace elements (Al, Si, Ti, P, Ba, Cu, Ni, Zr, Mo) were measured in 240 hand and powdered samples with a Bruker Trace III (Appendix A).

Shale samples for HHXRF analysis were prepared by breaking off small pieces of each sample and cleaning off excess dust or debris with water and allowing to dry completely before further processing. The small shale pieces were gently crushed with a mortar and pestle until a fine powder was obtained and placed in a small plastic container for analysis. The mortar and pestle were cleaned between each sample with water and rubbing alcohol to avoid contamination. Chert samples that were too hard to crush by hand were broken down into small, ~1-2 cm, fragments by placing the samples between two pieces of clean paper and smashing with a rock hammer. The small chert fragments were then placed in an alumina shatterbox and pulverized for eight minutes until a fine powder was obtained. For the sake of time, most chert samples were cut with a tile saw, to give a fresh surface to record measurements from, and polished with sandpaper to remove any excess metal from the tile saw.

The samples were analyzed at Kansas State University with a Bruker Trace III Hand-Held X-Ray Fluorescence instrument following methods developed by Rowe et al. (2012). Major elements were run for 180 seconds, under a vacuum, with no filter at 15 kV and 25 μ A, whereas trace elements were run for 120 seconds, with no vacuum, and using the yellow filter at 40kV and 12.4 μ A. Each sample was run three times and the calculated averages of each sample were used as final concentrations. Averaging the measurements was used to account for the heterogeneity that any one sample may have, allowing for more representative measurements of each sample. A standard mudrock sample, RTC-WS-220, was run between every 6 measurements to ensure there was no variation in the machine's operation. Standard

measurements can be found in Appendix A. Sample concentrations were calculated using the Bruker Mudrock calibration. A full table of the concentrations obtained for both major and trace elements can be found in Appendix A. To account for any drift of the equipment during analysis, further normalization was performed for each element by comparing the Woodford standard (RTC-WS-220) with accepted values from Rowe et al. (2012). A table containing Rowe's values along with our calculations can be found in Appendix A.

Elemental concentrations were normalized to aluminum (e.g., Si/Al) to subtract possible variations in the sedimentation rate, which ultimately may dilute the trace-element concentrations (Tribovillard et al., 2006). For this study, Si, Ti and Zr were used as proxies for detrital input, since they are commonly found in detrital sources (Tribovillard et al., 2006). Mo and U were used as proxies for degree of oxygenation, since the removal of these elements as oxyhydroxides under anoxic conditions results in enrichments of several orders of magnitude above detrital values (Tribovillard et al. 2006; Arnaboldi and Meyers, 2007; Algeo and Maynard, 2008). Fe was also used as a proxy for degree of oxygenation as a result of enrichment in ancient euxinic environments (Lyons and Severmann, 2006). Ba, Cu, and Ni served as proxies for primary productivity, as these elements are either released during phytoplankton/OM decay or act as nutrients in oxic settings (Tribovillard et al., 2006), although Cu and Ni also tend to be enriched in anoxic environments. P was also used as indicative of primary productivity, as it often reflects phosphate accumulation (Tribovillard et al., 2006). The behavior (e.g., variable or constant) and value trends (increasing or decreasing) in these indices, along with the facies analysis, were used to interpret the depositional conditions and identify sequences and systems tracts, and ultimately interpret the controlling mechanisms in the accumulation of organics within the Woodford.

Total organic carbon and sulfur

Total organic content (TOC) was measured in 10 samples (Table 2) through LECO carbon analysis by GeoMark Research in Humble, TX. These 10 samples were chosen from different sections of the outcrop and represent the lithofacies described in Table 1.

Table 2: Carbonate, Total Organic Carbon (TOC), and Sulfur weight % for samples from I-35 outcrop.

Sample	Percent carbonate (wt%)	TOC (wt%)	Sulfur (wt%)	Sequence
OK-1-12	6.86	12.90	2.36	1
OK-1-33	4.48	11.90	0.91	1
OK-1-68	10.61	7.02	2.35	2A
OK-1-84	5.32	10.60	1.57	2A
OK-1-116	4.90	12.10	1.32	2B
OK-1-129	5.49	12.70	1.55	2B
OK-1-155	9.06	14.40	1.16	3A
OK-1-193	6.52	20.90	1.93	3A
OK-1-214	37.12	7.58	2.19	3B
OK-1-235	5.72	2.17	0.28	3B

Inductively-coupled plasma mass spectrometry (ICP-MS)

U and Mo (among 29 other elements) concentrations were obtained for 10 samples (Table 3) by inductively-coupled plasma mass spectrometry (ICP-MS) at WSU GeoAnalytical Lab, School of Environment at Washington State University. Data obtained by this analysis allowed for the comparison of Mo concentrations between HHXRF and ICP-MS, which is used to test the accuracy of the HHXRF measurements.

Table 3: ICP-MS data for samples from the I-35 outcrop.

Sample ID	La ppm	Ce ppm	Pr ppm	Nd ppm	Sm ppm	Eu ppm	Gd ppm	Tb ppm	Dy ppm	Ho ppm	Er ppm	Tm ppm	Yb ppm	Lu ppm	Ba ppm	Th ppm
OK-1-12	59.84	106.50	13.11	52.35	10.43	2.14	6.95	0.60	2.71	0.46	1.11	0.15	0.90	0.14	4556	6.99
OK-1-33	24.67	42.68	5.60	22.12	4.26	0.79	2.62	0.29	1.59	0.33	0.90	0.13	0.81	0.13	786	4.93
OK-1-68	6.68	12.07	1.49	5.66	1.35	0.31	1.79	0.33	2.17	0.47	1.27	0.19	1.14	0.18	662	1.84
OK-1-84	18.83	31.67	4.37	16.92	3.36	0.67	2.73	0.37	2.31	0.49	1.37	0.20	1.27	0.19	705	4.35
OK-1-116	17.66	26.81	4.09	15.08	2.73	0.50	1.91	0.29	2.02	0.45	1.53	0.25	1.68	0.29	579	5.46
OK-1-129	21.07	29.16	4.55	16.82	2.64	0.52	1.97	0.27	1.76	0.43	1.37	0.22	1.50	0.25	692	5.00
OK-1-155	24.31	44.58	6.52	27.18	5.90	1.25	4.79	0.60	3.19	0.61	1.65	0.24	1.43	0.22	843	5.23
OK-1-193	18.30	26.77	4.96	19.35	3.01	0.46	1.54	0.22	1.25	0.25	0.72	0.12	0.85	0.14	1083	4.54
OK-1-214	72.15	88.38	22.33	107.16	29.05	6.83	34.58	5.21	30.43	6.13	15.05	1.86	10.06	1.54	1121	2.31
OK-1-235	9.98	11.09	2.58	10.89	2.47	0.61	2.97	0.47	2.90	0.63	1.77	0.25	1.50	0.25	1254	0.95

Sample ID	Nb ppm	Y ppm	Hf ppm	Ta ppm	U ppm	Pb ppm	Rb ppm	Cs ppm	Sr ppm	Sc ppm	Zr ppm	Ni ppm	Mo ppm	Co ppm	Cu ppm
OK-1-12	10.22	13.17	2.98	0.68	26.85	4.64	87.1	5.02	837	6.1	114	65.6	127.9	2.88	26.43
OK-1-33	8.70	9.28	2.19	0.56	22.06	9.00	89.7	5.77	106	6.6	81	81.1	122.2	2.89	18.63
OK-1-68	3.99	16.01	1.05	0.26	24.79	1.09	43.6	2.38	63	2.8	39	61.0	36.8	10.34	54.24
OK-1-84	5.42	15.72	1.51	0.36	16.55	2.83	62.2	4.00	88	4.9	56	70.0	184.8	2.79	34.40
OK-1-116	6.85	15.23	1.95	0.49	17.75	3.98	89.0	5.92	65	6.1	72	70.5	163.9	2.48	21.49
OK-1-129	6.28	13.60	1.74	0.45	30.95	3.62	84.1	5.57	91	6.3	67	84.0	135.1	2.51	38.09
OK-1-155	6.13	19.58	1.58	0.41	47.25	8.80	63.2	4.25	173	5.3	63	73.4	205.1	2.17	30.32
OK-1-193	4.69	7.00	1.34	0.32	16.68	4.26	70.2	4.94	148	6.9	50	113.6	156.1	2.36	181.07
OK-1-214	1.59	205.50	0.55	0.10	180.71	5.29	14.4	0.84	1615	10.8	28	544.6	115.7	14.98	63.28
OK-1-235	1.20	24.17	0.35	0.07	8.97	6.92	7.9	0.48	469	2.3	16	47.2	5.3	1.21	30.10

X-ray diffraction (bulk analysis)

X-ray diffraction (XRD) analysis was performed at Kansas State University for eight samples to determine the bulk composition of mudrocks. These eight samples consisted of each of the lithofacies identified in the outcrop and were collected in evenly spaced intervals (~10 ft) to ensure a fair representation of the entire outcrop.

Samples were processed by first cleaning and drying the samples to remove excess dust. They were then crushed between two pieces of clean paper into small, ~1-2 cm, pieces that were powdered by using a mortar and pestle, cleaned with water, and rubbing alcohol between each sample to reduce contamination.

The sample powders were then pressed into a cylindrical container with a diameter of 27 mm and analyzed in a PANalytical Empyrean Series 2 X-ray diffractometer. The sample powders were scanned between two theta values of 5 and 70 degrees. Diffractograms were produced using the software HighScore Plus that allowed for mineral peaks to be identified.

Data integration

Integration of the sedimentological log alongside the data from TOC, XRD, ICP-MS and HHXRF elemental concentrations analyses allow us to look at the variation in these parameters and interpret if they reflect allogenic controls throughout the stratigraphic succession. The behavior of the previously listed parameters allowed for the separation (using parameters such as changes in grain size and chemical indices) of the otherwise homogenous-looking outcrop into different sequences and subsequences shown in Figure 4. Finally, the identification of these controls in intervals of high organic concentration helped in constraining the main drivers in organic accumulation within the Woodford, discussed in Chapter 5.

Chapter 4 - Results

Facies analysis

Four lithofacies were identified and refined with the aid of petrography: organic shale (ShO), radiolarite (R), siliceous shale (ShR), and intraformational conglomerate (Ci)) (Table 1). ShO and R facies are interpreted as deep marine deposits formed by settling of planktonic organisms (algae and radiolarians) in distal settings with varying conditions of primary productivity (Stow and Smillie, 2020; Loucks and Ruppel, 2007). ShR is interpreted as a hemipelagic deposit formed from alternated settling of mud delivered by surface plumes (low-density turbidites) or wind mixed with pelagic fallout (Peng, 2021; Talling et al., 2012). Hemipelagic settling occurs in shallower, slope settings where sediments settle vertically and are reworked laterally within the water column (Stowe and Smillie, 2020). The lateral reworking can be the result of river plumes, glacial meltwater diffusion, or turbid layer plumes (Stow and Smillie, 2020).

These lithofacies were grouped in two facies associations (pelagic and hemipelagic marine). Pelagic marine deposits are dominated ShO and R facies whereas hemipelagic marine deposits are composed of ShR and R facies. These two facies associations represent variable water depths where pelagic deposits represent the deepest marine settings. The sedimentary succession in the studied outcrop shows a change from dominantly pelagic deposits at the base, to alternating pelagic and hemipelagic in the middle section, to dominantly hemipelagic deposits at the top. This suggests a shallowing trend in the basin, despite the overall deep-water environment where these sediments accumulated.

Chemostratigraphic analysis and stratigraphic framework

The succession exposed on the I-35 outcrop can be split into three main sequences, with Sequences 2 and 3 being subdivided into two further sections, A and B (Fig. 4). The three main

sequences were determined based on patterns and changes in the sedimentologic characteristics (clay-rich vs. quartz-rich) and behavior of chemical indices (detrital input, primary productivity, degree of oxygenation), while the subdivisions of Sequences 2 and 3 were based specifically on changes in the proxies for primary productivity and degree of oxygenation.

Sequence 1 is found within lowermost 17 feet of the I-35 outcrop (Fig. 4). Grain sizes in Sequence 1 range from medium-to-coarse mud. The base of Sequence 1 is defined by alternating, 1-3 ft, packages of organic rich shale (ShO) interbedded by 3-6-inch Radiolarite (R) deposits. This alternation continues until ~12 ft from the base of the outcrop, where fine, centimetric interbedding of ShO and R begins. Detrital (Si/Al, Ti/Al, Zr/Al) and productivity (Ba/Al, P/Al, Ni/Al, Cu/Al) proxies have constant, low values overall throughout Sequence 1, except for localized peaks in Si/Al, Zr/Al, Ba/Al and P/Al (e.g. ~ 8 ft and 12 ft). The peaks in detrital and productivity logs match areas of the sedimentary log where Radiolarite deposits are the primary facies. Ti/Al peaks in the first 8 feet of the sequence are a mirror image of the other detrital proxy peaks. From 8 feet upward, Ti/Al behaves the same as the Si/Al and Zr/Al indices. Mo/Al is also low and constant, whereas Fe/Al values are the highest in the entire log within Sequence 1, and Fe/Al is highly variable.

Sequence 2 spans from ~17ft to ~53 ft in the outcrop (Fig. 4). The lithology of Sequence 2 includes ShO, R, and radiolarian-rich shale (ShR) deposits. R and ShO deposits are evenly and repetitively interbedded from 17-44 feet in the section. At 44 feet, the average bedding thickness for ShO and R becomes much smaller (~3 inches to 1.5 inches). From 37 to 48 feet, silica nodules occur within the R beds. Detrital proxy values in Sequence 2 are low overall, but much more variable than in Sequence 1, with peaks usually coinciding with layers where silica content is higher (R and ShR beds). All detrital proxies tend behave the same throughout Sequence 2, except for the intervals of 18-23 ft and

48-53 ft, where Ti/Al is opposite to Si/Al and Zr/Al. Productivity proxies are highly variable throughout Sequence 2, with peaks in Ba/Al and P/Al usually coinciding with peaks in the detrital proxies. The behavior of Ni/Al and Cu/Al changes halfway through Sequence 2, which guided the subdivision into sections A (lower half of the sequence) and B (upper half of the sequence). Sequence 2A is defined by consistently low values in primary productivity and degree of oxygenation proxies. At ~35 ft, the proxies display more variation, marking the beginning of Sequence 2B. This change coincides with the appearance of silica nodules.

The base of Sequence 3 is marked by the occurrence of an intraformational conglomerate (Ci) of ~1ft thickness composed of R and ShO clasts (Fig. 4). Overlying this layer is a thin interbedding of R and ShO ~1 inch in thickness each. Silica nodules are also abundant in this sequence and are found in most R layers. All indices in Sequence 3 are highly variable and with the highest overall values. The increase in elemental ratio values coincides with the appearance of the intraformational conglomerate in the sedimentary log. Detrital proxies (Si/Al, Ti/Al, Zr/Al) peak with silica rich (R facies) layers in the section. Detrital proxies show the same behavior throughout the sequence, except for a brief interval at 77 ft where Ti/Al decreases as Si/Al and Zr/Al increase. Productivity and degree of oxygenation proxies do not coincide with detrital proxies. The different behavior of the productivity and degree of oxygenation proxies allows for the subdivision of Sequence 3 into two sections. Sequence 3A (the lower two-thirds of the section) is defined by constant, low Fe/Al, Ni/Al, and Mo/Al indices and high, variable Cu/Al values. At ~71 feet in the section, there is an increase in values and variability in Fe/Al, Ni/Al, and Mo/Al and a change in Cu/Al to consistently low values. This break defines the beginning of sequence 3B.

Carbonate, total organic carbon, and sulfur analysis

Carbonate, total organic carbon (TOC), and sulfur wt% were obtained from 10 samples (Table 2). Carbonate percentages among the 10 samples range from 4.48-6.86 wt%, except for samples OK-1-68 and OK-1-214 which have carbonate concentrations of 10.61 and 37.12 wt%, respectively. TOC concentrations were very high (relative to the average shale), with most samples between 11.90 and 14.40 wt%, except samples OK-1-68 (7.0 wt%), OK-1-193(20.90 wt%), OK-1-214 (7.58 wt%), and OK-1-235 (2.17 wt%). Lastly, sulfur concentrations among the samples falls between 0.28 and 2.36 wt%.

XRD bulk analysis

XRD diffractograms for bulk rock were obtained for five samples (OK-1-1, OK-1-8, OK-1-57, OK-1-131, OK-1-222) (Appendix B). All of the diffractograms are very similar and show that the samples selected from the outcrop are composed primarily of quartz (Fig. 5).

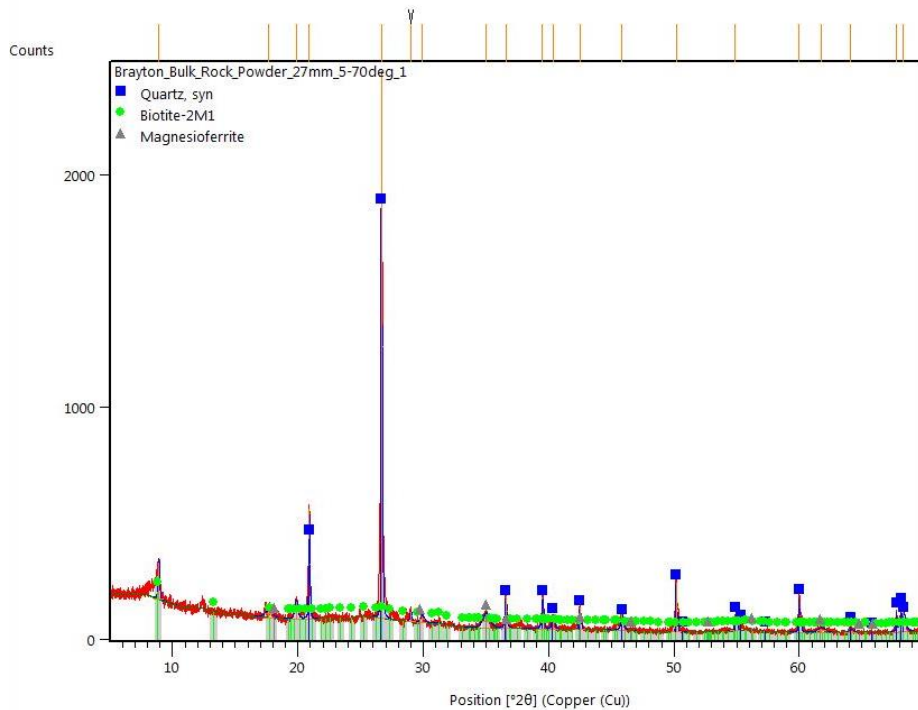


Figure 5: Diffractogram (bulk analysis) for sample OK-1-1. Major peaks match with those of quartz, biotite, and magnesioferrite.

Inductively-Coupled Plasma Mass Spectrometry

ICP-MS analysis was performed for the same 10 samples listed in Table 2, where 31 elemental concentrations were measured (Table 3). ICP-MS data was used to check the accuracy of HHXRF measurements of Mo (Fig. 6).

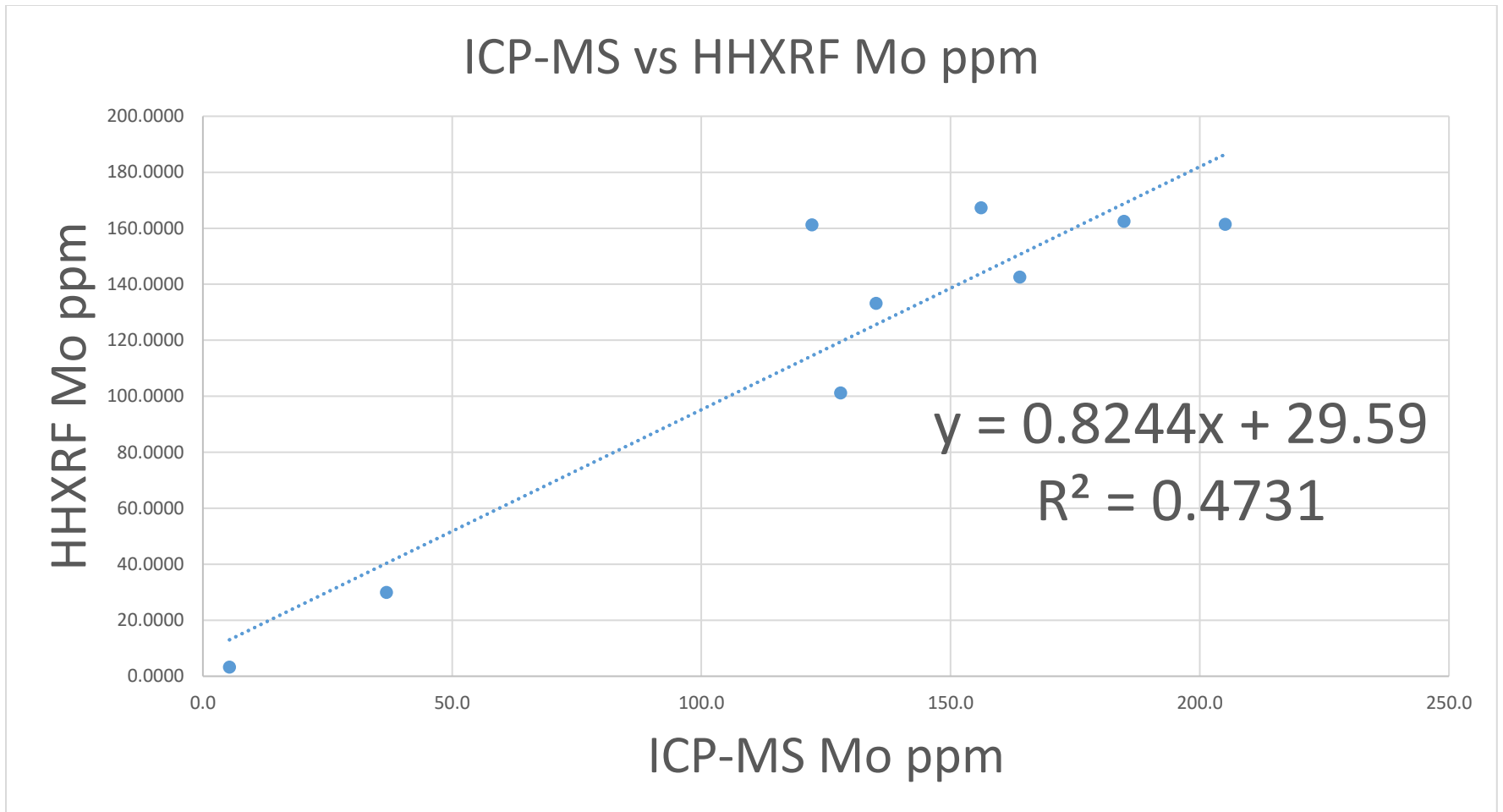


Figure 6: ICP-MS vs HHXRF concentration of Mo (in ppm)

Chapter 5 - Discussion

Sequence 1 consists of a succession of organic-rich shales and radiolarites and shows relatively low and constant indices, except for a few localized elemental concentration peaks at ~7 and 12 ft, suggesting an overall stable system with constant sedimentation rate, primary productivity, and degree of oxygenation in the bottom waters. The highest peaks are seen in the detrital indices (Zr/Al and Si/Al), which match the peaks found in the productivity indices (Ba/Al and P/Al). Si/Al can be related to either detrital or biogenic flux, so it alone would not suggest whether high Si/Al value is related to higher sedimentation rates or productivity due to increased nutrient supply (Sageman and Lyons, 2004). Abundant radiolarians and Tasmanites found in samples from Sequence 1 suggest primary productivity was prevalent, leading to higher concentrations of organic matter in the sequence (Figs. 7 and 8). Radiolarians and biogenic chert are indicative of upwelling and high productivity environments (Kidder and Erwin, 2001). The other detrital proxy, Ti/Al, shows reverse peaks to Si/Al and Zr/Al (e.g., decreasing Ti/Al with increasing Si/Al), which suggest that increased Si/Al values are related to increased productivity, since Ti/Al increase are associated with either tectonic or eolian processes bringing detrital sediments into the system (Sageman and Lyons, 2004). Mo/Al in Sequence 1 is low and constant, suggesting oxic bottom waters. Likewise, productivity proxies, being low and constant (except for localized peaks), indicate an overall low organic flux. High Fe/Al is usually attributed to euxinic or anoxic environments, where there is little to no oxygen and an abundance of sulfur (in euxinic environments) leading to pyrite mineralization, and low siliciclastic input is observed (Lyons and Severmann, 2006). Other indications of anoxia in Sequence 1 include TOC wt% measuring 12.9 and 11.9% and enrichment factors for U and Mo greater than 16 (Goldberg and Humayun, 2016). Fe/Al variability does not appear to coincide either with detrital or productivity indices. Enrichment factors for Ni, Cu, and U in Sequence 1 are the lowest in the entire succession, although enriched more than 10

times the average shale (enrichment is defined by enrichment factors – $EF > 1$, according to Tribovillard et al., 2006; minimum and maximum EF in the studied succession for Cu = 9.2/10.44, Ni = 3.30/44.41, U = 168.76/198.17), indicative of an anoxic environment (Goldberg and Humayun, 2016). In summary, the bottom-water conditions during the sedimentation of Sequence 1 are not entirely clear, but Fe/Al coupled with high TOC and the enrichment factors for U and Mo, suggests that conditions were primarily anoxic, possibly euxinic. Primary productivity was overall low, with peaks associated with riverine input of nutrients, as suggested by the coincidence between detrital and productivity proxies. The presence of stagnant waters is compatible with the scenario described above.

Sequence 2 transitions from mainly pelagic to hemipelagic facies (ShR and R facies), with low and variable detrital, productivity, and degree of oxygenation indices. Sequence 2 is subdivided into two sections, A and B, based on changing values of productivity indices (Ni/Al and Cu/Al increase at 35ft). Sequence 2A detrital peaks match productivity peaks (e.g. at 22 and 28 ft), suggesting that detrital input and riverine nutrient supply are major controls on productivity in this sequence. Differently from Sequence 1, the detrital index Ti/Al behaves the same as Si/Al and Zr/Al throughout, possibly reflecting an increase in eolian flux or riverine input (Sageman and Lyons, 2004). Degree of oxygenation indices in 2A are low and have little variation, suggesting stable, more oxic settings compared to Sequence 1. TOC in two samples from Sequence 2A are 7.02% and 10.60 wt%, slightly lower than those from Sequence 1, in agreement with slightly more oxic conditions leading to oxidation of organics. Detrital input seems to have been responsible for riverine nutrient input (and resulting increase in primary productivity) but also oxygenation of bottom waters. Ni/Al and Cu/Al ratios suggest that primary productivity was somewhat low during the deposition of Sequence 2A.

Sequence 2B is characterized by an even mix of hemipelagic and pelagic deposits and the first appearance of silica nodules in the ShR and R facies. There is a decline and short intervals of constant

ratios for Si/Al in 2B, while Ti/Al and Zr/Al ratios are similar to 2A measurements. There is an increase in productivity indices (Ba/Al, Ni/Al and Cu/Al) in Sequence 2B, suggesting an increasing in organic flux relative to sequences 1 and 2A. Enrichment factors in Ni, Mo and U are high in Sequence 2B (average $EF_{Ni} = 16$, $EF_{Mo} > 200$, $EF_U > 13$, in comparison to average $EF_{Ni} = 13$, $EF_{Mo} > 38$ and $EF_U > 13$ in Sequence 2A), pointing to anoxic conditions. However, it should be noted that U and Mo are comprised of two data points. Sequence 2B also contains samples with abundant radiolarians, Tasmanites, and plant matter, supporting a high-productivity anoxic setting ideal for organic matter preservation, with some terrestrial contribution. TOC from two samples taken from a pelagic interval in Sequence 2B is 12.10 and 12.70 wt%, similar to those from pelagic deposits in Sequence 1.

Sequence 3 is primarily hemipelagic deposits consisting of ShR and R facies that is further divided into two subsequences, A and B. Sequence 3A is defined by the highest and most variable detrital and primary productivity indices of the entire outcrop, except for Ni/Al (low and constant) while having low degree of oxygenation indices. The detrital peaks coincide with the large peaks in productivity in the section, suggesting that riverine input is a major control on nutrient supply in this highly productive environment. Degree of oxygenation indices would suggest that the bottom waters during deposition of Sequence 3A were mostly oxic, with short-lived intervals of anoxia. TOC in samples from a pelagic and a hemi-pelagic deposit in Sequence 3A is 14.40 and 20.40 wt% respectively, comprising the highest TOC in the entire section. This suggests that increased primary productivity triggered by riverine input (in other words, organic flux) is a more important control in the burial of organics in the sediments than anoxia.

Sequence 3B consists of R and ShO facies, comprising primarily of pelagic deposits, with smaller intervals of hemipelagic deposits at the base and top. Sequence 3B marks a drop in detrital and productivity indices (except for Ni/Al, the highest in the studied section, minimum and maximum Ni/Al

= 0.003/0.04), but an increase in degree of oxygenation indices, with the highest Mo/Al in the succession, indicating a productive, anoxic environment (Tribovillard et al., 2006). TOC from two samples in Sequence 3B is 7.58 and 2.17 wt%, measured in a hemipelagic and a pelagic deposit, respectively. Despite high TOC, these are the samples with the lowest organic content of all samples throughout the entire succession, somewhat surprising given the indication of high primary productivity provided by Ni/Al and anoxia suggested by Mo/Al. Therefore, other factors not detected by these analyses may be controlling the burial of organics in the uppermost Woodford Shale in the I-35 outcrop.

A possible explanation is that upwelling may not have been an effective way of providing nutrients during the succession's deposition. Paleogeographic reconstructions of the study area would suggest that equatorial upwelling was likely to occur in the area. However, increases in global temperatures during the late Devonian and early Carboniferous (Scotese et al., 2021) may have caused weaker winds that would result in less effective upwelling. The overall coincidence between high detrital input and high productivity indicated by chemical indices suggests that riverine nutrient input played a role in boosting primary productivity, resulting in higher organic flux and burial in the sediments.

The three sequences and their subsequences exposed in the I-35 outcrop were deposited in a deep marine environment under variable conditions. Deposition of Sequence 1 occurred under stable anoxic-euxinic conditions with low to moderate productivity, the main control on organic content being enhanced preservation, perhaps related to stratification in the water column resulting in a stagnant setting. During deposition of Sequence 2A, primary productivity did not change substantially from Sequence 1, but shallowing led to increased oxygenation of the bottom waters, resulting in lower organic content due to enhanced oxidation. Sedimentation of Sequence 2B was characterized by the same bottom-water conditions but with increased primary productivity, resulting in higher organic

burial. Sequence 3A was deposited in a shallower environment with the highest detrital input and primary productivity. The fact that this sequence contains the highest concentration of organics in the studied succession suggests that primary productivity (boosted by riverine nutrient input) was the main control in the burial of organic matter, even in the absence of persistently anoxic conditions. These conditions suggest that organic flux plays a larger role than anoxia during the burial of organics in the sediments. Finally, Sequence 3B was deposited under strongly anoxic conditions but not particularly high productivity, which resulted in the lowest organic content in the studied succession.

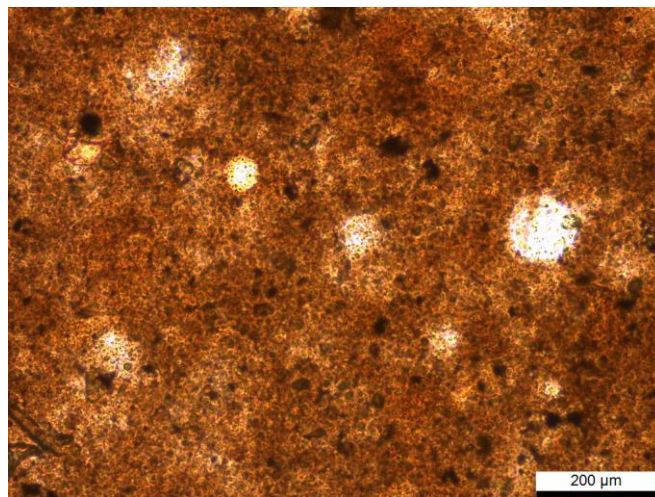


Figure 7: Photomicrograph of radiolarians (white circles) and pyrite (black clusters) found in samples from Sequence 1.

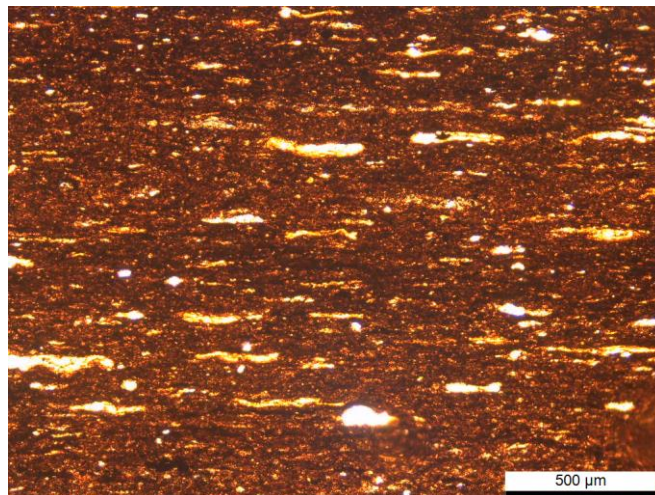


Figure 8: Photomicrograph of Tasmanites (thin orange bioclasts) immersed in clay matrix with scattered fine quartz grains (Sequence 1).

Chapter 6 - Conclusions

The I-35 Woodford Shale outcrop can be divided into three main sequences (1, 2, and 3, from base to top), with sequences 2 and 3 further subdivided into subsequences (A and B), based on changes in chemostratigraphic indices proxies for detrital input, primary productivity, and degree of oxygenation, and accompanied facies associations. Sequence 1 is characterized by distal, pelagic settling sediments with 12-13 wt% TOC deposited under conditions of stable anoxia/euxinia, with low-moderate primary productivity. Sequence 2A is defined by interbedded pelagic and hemipelagic deposits with TOC between 7-11 wt%. It was deposited in more oxic environments because of decreased water depths, resulting in less preservation of organics. The continued accumulation of pelagic and hemipelagic deposits in Sequence 2B is accompanied by increased primary productivity following an increase in nutrient supply from upwelling and continental waters, which resulted in organic contents of about 12 wt%. The hemipelagic deposits of Sequence 3A display the highest TOC in the entire succession (14-20 wt%), as a consequence of productivity boosts due to riverine nutrient input, despite the presence of overall oxic bottom waters with occasional anoxic events. Sequence 3B accumulated in a low to moderately productive environment under strongly anoxic conditions, resulting in the lowest TOC in the entire section (2-8 wt%).

The detailed study of the I-35 Woodford Shale outcrop indicates that high organic content (TOC>10%) is found in settings where primary productivity is high, regardless the bottom-water conditions. Primary productivity was boosted by riverine nutrient input associated with shallowing waters. The results of this study suggest that organic flux is more important than anoxia in the burial of organics in the sediments, with anoxia oftentimes being a consequence of high organic flux.

References

- Algeo, T. J., & Maynard, J. B. (2008). Trace-metal covariation as a guide to water-mass conditions in ancient anoxic marine environments. *Geosphere*, 4(5), 872–887.
<https://doi.org/10.1130/GES00174.1>
- Arnaboldi, M., & Meyers, P. A. (2007). Trace element indicators of increased primary production and decreased water-column ventilation during deposition of latest Pliocene sapropels at five locations across the Mediterranean Sea. *Paleogeography, Palaeoclimatology, Paleoecology*, 249(3–4), 425–443.
- Balter, V., Renaud, S., Girad, C., & Joachimski, M. M. (2008). Record of climate-driven morphological changes in 376 Ma Devonian fossils. *Geological Society of America*, 36(11), 907–910.
- Basilone, L., Frixia, A., Trincianti, E., & Valenti, V. (2016). Permian-Cenozoic deep-water carbonate rocks of the Southern Tethyan Domain. The case of Central Sicily. *Italian Journal of Geosciences*, 135(2), 171–198.
- Brezniski, K. D., Cecil, B. C., Skema, W. V., & Stamm, R. (2008). Late Devonian glacial deposits from the eastern United States signal an end of the mid-Paleozoic warm period. *Paleogeography, Paleoclimatology, Paleoecology*, 268(1), 143–151.
- Brezniski, K. D., Cecil, B. C., & Skema, W. V. (2010). Late Devonian glacial and associated facies from the central Appalachian Basin, eastern United States. *GSA Bulletin*, 122(1), 265–281.
- Brower, S. (2019). *An integrated sedimentological-chemostratigraphic study of the Late Devonian-Early Mississippian Chattanooga Formation in Kansas: High-resolution stratigraphy and organic matter accumulation*. Kansas State University.
- Calvert S.E., Pedersen T.F. (1992). Organic carbon accumulation and preservation in marine sediments: how important is anoxia? In: Whelan J.K., Farrington J.W. (eds.) *Organic matter: Productivity, accumulation, and preservation in recent and ancient sediments*, New York, Columbia University Press, p. 231-263.
- Collison, J.D. (1996) Alluvial Sediments. In: Reading, H.G., Ed., *Sedimentary Environments: Processes, Facies and Stratigraphy*, 3rd Edition, Blackwell Science, Oxford, 37-81.
- Comer, J. B. (2008). *Woodford Shale in Southern Midcontinent, USA- Transgressive System Tract Marine Source Rocks on an Arid Passive Continental Margin with Persistent Oceanic Upwelling*.
- Flügel, E. (2010). *Microfacies of carbonate rocks: Analysis, interpretation, and application* (2nd ed.). Springer.

- Goldberg, K., & Humayun, M. (2016). Geochemical paleoredox indicators in organic-rich shales of the Irati Formation, Permian of the Parana Basin, southern Brazil. *Brazilian Journal of Geology*, 46(3), 377–393.
- Harris, D. M. (2017). *A laboratory investigation into rock physics and fracture potential of the Woodford shale, Anadarko Basin, Oklahoma*. Kansas State University.
- Hemmesch, N. T., Harris, N. B., Mnich, C. A., & Selby, D. (2014). A sequence-stratigraphic framework for the Upper Devonian Woodford Shale, Permian Basin, West Texas. *AAPG Bulletin*, 98(1), 23–47.
- Housenknecht, W. D., Rouse, A. W., Paxton, S., Mars, C. J., & Fulk, B. (2014). Upper Devonian–Mississippian stratigraphic framework of the Arkoma Basin and distribution of potential source-rock facies in the Woodford–Chattanooga and Fayetteville–Caney shale-gas systems. *AAPG Bulletin*, 98(9), 1739–1759.
- Kidder, D. L., & Erwin, D. H. (2001). Secular Distribution of Biogenic Silica through the Phanerozoic: Comparison of Silica-Replaced Fossils and Bedded Cherts at the Series Level. *The Journal of Geology*, 109(4), 509–522.
- James, N. P., & Dalrymple, R. W. (2010). Facies models 4. Geological association of Canada
- Janssen, K. W. (2017). *A study of the effects of organic matter on illitization in the Woodford Shale, Oklahoma and Kansas*. Kansas State University.
- Krystyniak, A. (2005). *Outcrop-Based Gamma-Ray Characterization of the Woodford Shale of South-Central Oklahoma*. Oklahoma University.
- Lambert, M.W. (1993). Internal Stratigraphy and Organic Facies of the Devonian-Mississippian Chattanooga (Woodford) Shale in Oklahoma and Kansas: Chapter 11.
- Li, Y., & Schieber, J. (2015). On the Origin of a Phosphate Enriched Interval in the Chattanooga Shale (Upper Devonian) of Tennessee—A Combined Sedimentologic, Petrographic, and Geochemical Study. *Sedimentary Geology*, 329, 40–61.
- Loucks, R. G., & Ruppel, S. C. (2007). Mississippian Barnett Shale: Lithofacies and depositional setting of a deep-water shale-gas succession in the Fort Worth Basin, Texas. *AAPG Bulletin*, 91(4), 579–601.
- Lyons, T. W., & Severmann, S. (2006). A critical look at iron paleoredox proxies: New insights from modern euxinic marine basins. *Geochimica et Cosmochimica Acta*, 70(23), 5698–5722.
<https://doi.org/10.1016/j.gca.2006.08.021>
- McColloch, A. (2016). *Distribution and source rock potential of the Chattanooga Shale in Kansas*. Kansas State University.

- Parrish, J. T., & Curtis, R. L. (1982). Atmospheric circulation, upwelling, and organic-rich rocks in the Mesozoic and Cenozoic eras. *Paleogeography, Palaeoclimatology, Paleocology*, 40(1–3), 31–66.
- Peng, J. (2021). Sedimentology of the Upper Pennsylvanian organic-rich Cline Shale, Midland Basin: From gravity flows to pelagic suspension fallout. *Sedimentology*, 68(2), 805–833. <https://doi.org/10.1111/sed.12811>
- Pope, C. M., & Steffen, B. J. (2003). Widespread, prolonged late Middle to Late Ordovician upwelling in North America: A proxy record of glaciation?. *Geological Society of America*, 31(1), 63–66.
- Raymond, A., & Metz, C. (2004). Ice and Its Consequences: Glaciation in the Late Ordovician, Late Devonian, Pennsylvanian-Permian, and Cenozoic Compared. *The Journal of Geology*, 112(6), 655–670.
- Rowe, H., Hughes, N., & Robinson, K. (2012). The quantification and application of handheld energy-dispersive x-ray fluorescence (ED-XRF) in mudrock chemostratigraphy and geochemistry. *Chemical Geology*, 324–325, 122–131. <https://doi.org/10.1016/j.chemgeo.2011.12.023>
- Schieber, J. (1998). Developing a sequence stratigraphic framework for the Late Devonian Chattanooga Shale of the Southeastern U.S.A.: Relevance for the Bakken Shale. *Saskatchewan Geological Society*, 13(1), 58–68.
- Scotese, C. R., Song, H., Mills, B. J. W., & van der Meer, D. G. (2021). Phanerozoic paleotemperatures: The earth's changing climate during the last 540 million years. *Earth-Science Reviews*, 215, 103503. <https://doi.org/10.1016/j.earscirev.2021.103503>
- Slatt, R. M., Buckner, N., Younane, A., Sierra, R., Philp, P. R., Miceli-Romero, A., Portas, R., O'Brien, N., Tran, M., Davis, R., & Wawrzyniec, T. (2012). Outcrop-behind Outcrop (Quarry) Multiscale Characterization of the Woodford Gas Shale, Oklahoma. In J. A. Breyer, *Shale Reservoirs—Giant Resources for the 21st Century*. American Association of Petroleum Geologists. <https://doi.org/10.1306/13321481M97441>
- Stow, D. A. V., Huc, A.-Y., & Bertrand, P. (2001). Depositional processes of black shales in deep water. *Marine and Petroleum Geology*, 18(4), 491–498. [https://doi.org/10.1016/S0264-8172\(01\)00012-5](https://doi.org/10.1016/S0264-8172(01)00012-5)
- Stow, D., & Smillie, Z. (2020). Distinguishing between Deep-Water Sediment Facies: Turbidites, Contourites and Hemipelagites. *Geosciences*, 10(2), 68. <https://doi.org/10.3390/geosciences10020068>
- Talling, P. J., Masson, D. G., Sumner, E. J., & Malgesini, G. (2012). Subaqueous sediment density flows: Depositional processes and deposit types. *Sedimentology*, 59(7), 1937–2003. <https://doi.org/10.1111/j.1365-3091.2012.01353.x1>

- Tribovillard, N., Algeo, T. J., Lyons, T., & Riboulleau, A. (2006). Trace metals as paleoredox and paleoproductivity proxies: An update. *Chemical Geology*, 232(1–2), 12–32.
<https://doi.org/10.1016/j.chemgeo.2006.02.012>
- Turner, B. W., Tréanton, J. A., & Slatt, R. M. (2016). The use of chemostratigraphy to refine ambiguous sequence stratigraphic correlations in marine mudrocks. An example from the Woodford Shale, Oklahoma, USA. *Journal of the Geological Society*, 173(5), 854–868.
<https://doi.org/10.1144/jgs2015-125>
- Wehner, T. D. (2018). *Variations in Mineral Abundance within a Single Horizontal Well Path in the Woodford Shale, Arkoma Basin, Oklahoma*. Kansas State University.
- Woodrow, L. D., Fletcher, W. F., & Ahrnsbrak, F. W. (1973). Paleogeography and Paleoclimate at the Deposition Sites of the Devonian Catskill and Old Red Facies. *Geological Society of America*, 84(1), 3051–3064.

Appendix A - HHXRF Normalized Data

The procedure carried out to normalize our data included the following steps: 1) normalization of our standard values to Rowe et al. (2012) (please see below) between 20 standard runs (40 samples were measured for every 20 standard measurements), 2) calculation of the average of each element for every 20 runs, 3) division of the value obtained by Rowe et al. (2012) by the calculated average to obtain the normalization factor for elements in that run bracket, and 4) normalization of the initial measured element value.

Rowe et al. (2012) RTC-WS-220 Accepted/Measured Values										
Al	Si	Ti	Fe	P	Ni	Cu	Mo	Ba	Co	Zr
5.39	33.7	0.27	2.55	0.05	153	147	83	1884	No	95
wt%	wt%	wt%	wt%	wt%	ppm	ppm	ppm	ppm	data	ppm

Normalization example: Standards 1-20 have an average Al wt% of 5.54. The normalization for all Al for samples OK-1-1 to OK-1-40 is $5.39/5.54 = 0.973$. So, if sample OK-1-1 has an initial measured Al wt% of 5.30, then the normalized wt% of OK-1-1 is $5.30 \times 0.973 = 5.156$.

Normalization factors for elements										
Standard/Samples	Al	Si	Ti	Fe	P	Ni	Cu	Mo	Ba	Zr
STD 1-20 (OK-1-1 to OK-1-40)	0.973	1.004	0.988	0.948	0.495	1.136	1.343	1.130	0.906	0.856
STD 21-40 (OK-1-41 to OK-1-80)	0.974	0.999	0.962	0.896	0.472	1.138	1.337	1.116	0.952	0.859
STD 41-60 (OK-1-81 to OK-1-120)	0.988	0.993	0.967	0.896	0.469	1.125	1.325	1.135	0.951	0.854
STD 61-80 (OK-1-121 to OK-1-160)	0.998	1.000	0.971	0.895	0.482	1.144	1.338	1.126	0.890	0.857
STD 81-100	1.004	1.027	0.985	0.899	0.467	1.141	1.343	1.124	0.905	0.854

(OK-1-161 to OK-1-200)										
STD 101-120 (OK-1-201 to OK-1-240)	1.003	1.034	1.000	0.916	0.508	1.140	1.328	1.116	0.987	0.854

Normalized Major Elements (wt%)					
Sample	Al	Si	Ti	Fe	P
OK-1-1	5.156	26.931	0.315	1.321	0.027
OK-1-2	2.096	24.373	0.151	3.943	0.014
OK-1-3	3.981	25.651	0.283	1.617	0.035
OK-1-4	0.772	36.895	0.031	0.417	0.029
OK-1-5	3.479	25.851	0.272	0.813	0.023
OK-1-6	0.646	36.772	0.033	0.241	0.024
OK-1-7	4.203	18.995	0.292	6.254	0.024
OK-1-8	0.734	36.217	0.039	0.275	0.028
OK-1-9	2.856	20.392	0.185	3.334	0.030
OK-1-10	3.210	15.190	0.253	4.695	0.046
OK-1-11	3.926	21.849	0.264	4.313	0.053
OK-1-12	3.369	22.745	0.260	0.104	0.038
OK-1-13	3.167	21.573	0.271	0.917	0.062
OK-1-14	3.425	22.680	0.279	0.903	0.021
OK-1-15	3.502	26.063	0.272	1.063	0.022
OK-1-16	2.585	29.944	0.194	1.676	0.030
OK-1-17	2.823	27.684	0.223	1.843	0.027
OK-1-18	0.320	43.051	0.017	-0.218	0.039
OK-1-19	0.403	43.406	0.035	0.005	0.039
OK-1-20	1.562	33.816	0.136	1.263	0.026
OK-1-21	3.552	27.456	0.265	0.976	0.022

OK-1-22	3.995	26.400	0.286	2.183	0.025
OK-1-23	3.728	28.240	0.282	0.345	0.021
OK-1-24	1.356	28.087	0.079	3.116	0.013
OK-1-25	3.463	28.498	0.260	1.912	0.028
OK-1-26	0.756	36.156	0.045	-0.208	0.024
OK-1-27	3.514	28.348	0.259	0.793	0.024
OK-1-28	3.102	27.578	0.230	2.156	0.027
OK-1-29	0.286	41.977	0.023	-0.535	0.028
OK-1-30	3.536	27.475	0.258	1.664	0.024
OK-1-31	3.550	27.497	0.238	1.624	0.029
OK-1-32	2.021	26.612	0.140	0.044	0.019
OK-1-33	3.779	26.974	0.267	1.587	0.028
OK-1-34	0.617	38.892	0.032	0.015	0.030
OK-1-35	2.856	28.992	0.214	1.596	0.030
OK-1-36	0.674	35.639	0.037	-0.305	0.022
OK-1-37	1.329	43.330	0.091	1.572	0.037
OK-1-38	0.554	39.300	0.038	0.616	0.033
OK-1-39	0.941	38.327	0.056	2.992	0.055
OK-1-40	3.418	27.663	0.272	0.942	0.022
OK-1-41	1.074	40.691	0.049	3.693	0.029
OK-1-42	3.426	27.464	0.247	1.566	0.020
OK-1-43	3.645	29.775	0.297	0.716	0.024
OK-1-44	0.329	42.911	0.025	-0.369	0.031
OK-1-45	0.520	42.679	0.050	-0.118	0.030
OK-1-46	0.458	42.329	0.039	-0.242	0.029
OK-1-47	0.637	39.910	0.023	-0.209	0.022
OK-1-48	3.057	28.381	0.231	0.508	0.020
OK-1-49	2.968	29.841	0.237	0.454	0.020
OK-1-50	0.674	42.521	0.044	-0.368	0.031
OK-1-51	3.747	29.309	0.263	0.862	0.020

OK-1-52	0.410	41.378	0.023	0.048	0.027
OK-1-53	0.874	36.744	0.053	0.616	0.023
OK-1-54	3.402	27.251	0.262	1.360	0.024
OK-1-55	0.795	35.617	0.051	0.259	0.022
OK-1-56	3.108	27.667	0.253	0.738	0.025
OK-1-57	1.387	37.270	0.093	0.387	0.029
OK-1-58	0.400	42.099	0.025	0.158	0.035
OK-1-59	3.442	28.915	0.236	1.129	0.024
OK-1-60	3.499	27.150	0.267	2.128	0.025
OK-1-61	0.737	36.519	0.041	-0.587	0.024
OK-1-62	0.856	42.896	0.051	0.023	0.031
OK-1-63	3.464	30.114	0.219	0.790	0.033
OK-1-64	0.969	42.993	0.050	0.317	0.032
OK-1-65	0.782	42.659	0.038	0.122	0.032
OK-1-66	3.638	24.539	0.210	2.599	0.015
OK-1-67	0.784	34.190	0.038	-0.624	0.019
OK-1-68	5.032	25.840	0.237	2.574	0.037
OK-1-69	0.527	39.775	0.024	0.185	0.030
OK-1-70	2.886	24.470	0.184	0.249	0.018
OK-1-71	2.791	38.047	0.161	0.936	0.040
OK-1-72	1.055	41.771	0.087	0.210	0.036
OK-1-73	0.917	36.380	0.053	-0.044	0.027
OK-1-74	3.805	25.926	0.227	1.128	0.040
OK-1-75	1.090	38.586	0.061	0.197	0.032
OK-1-76	3.128	30.079	0.203	1.021	0.028
OK-1-77	0.337	44.222	0.031	0.372	0.057
OK-1-78	3.620	29.556	0.219	1.429	0.035
OK-1-79	2.751	27.249	0.178	0.476	0.025
OK-1-80	0.982	33.986	0.059	-0.897	0.021
OK-1-81	0.743	37.797	0.042	-0.028	0.030

OK-1-82	0.812	38.213	0.049	-0.624	0.029
OK-1-83	0.984	36.357	0.059	1.280	0.025
OK-1-84	2.696	29.517	0.176	0.133	0.027
OK-1-85	0.656	41.993	0.042	0.078	0.032
OK-1-86	0.454	42.737	0.024	1.089	0.039
OK-1-87	3.117	28.317	0.187	0.030	0.026
OK-1-88	0.629	41.517	0.039	0.004	0.032
OK-1-89	0.787	41.185	0.052	1.073	0.032
OK-1-90	3.079	30.816	0.182	-0.212	0.028
OK-1-91	0.843	37.323	0.043	0.134	0.025
OK-1-92	0.875	38.197	0.047	0.333	0.027
OK-1-93	0.870	38.857	0.043	0.144	0.033
OK-1-94	0.874	38.606	0.050	0.273	0.032
OK-1-95	2.779	25.358	0.169	0.056	0.018
OK-1-96	0.718	39.692	0.040	1.209	0.033
OK-1-97	3.564	28.395	0.225	-0.230	0.024
OK-1-98	0.564	35.165	0.027	0.027	0.022
OK-1-99	0.763	39.790	0.039	1.037	0.026
OK-1-100	3.089	26.388	0.218	1.027	0.026
OK-1-101	2.629	20.139	0.157	0.542	0.012
OK-1-102	0.813	4.732	0.054	-0.102	-0.003
OK-1-103	2.647	23.405	0.172	1.715	0.013
OK-1-104	3.550	28.259	0.245	2.604	0.025
OK-1-105	2.814	20.569	0.156	0.471	0.043
OK-1-106	2.538	39.162	0.142	-0.012	0.035
OK-1-107	0.609	42.522	0.036	1.318	0.037
OK-1-108	3.567	26.798	0.235	-0.255	0.021
OK-1-109	0.634	43.213	0.031	1.196	0.056
OK-1-110	3.927	24.735	0.230	1.173	0.020
OK-1-111	3.615	28.021	0.241	-0.136	0.031

OK-1-112	0.729	42.552	0.045	1.364	0.047
OK-1-113	3.581	29.139	0.227	-0.166	0.028
OK-1-114	0.570	40.203	0.028	1.862	0.033
OK-1-115	3.727	25.429	0.226	1.360	0.032
OK-1-116	3.983	27.160	0.252	1.272	0.027
OK-1-117	3.674	26.685	0.214	2.051	0.026
OK-1-118	3.650	24.760	0.226	-0.157	0.029
OK-1-119	0.665	41.908	0.052	-0.153	0.037
OK-1-120	0.558	42.368	0.038	1.153	0.038
OK-1-121	3.653	42.666	0.243	1.151	0.033
OK-1-122	3.465	27.100	0.248	1.511	0.032
OK-1-123	3.198	28.920	0.207	0.941	0.029
OK-1-124	3.442	28.398	0.181	0.937	0.029
OK-1-125	3.553	27.299	0.222	1.839	0.028
OK-1-126	3.493	27.007	0.202	1.633	0.030
OK-1-127	0.716	27.568	0.041	-0.100	0.042
OK-1-128	0.759	42.487	0.038	-0.010	0.045
OK-1-129	3.101	42.469	0.192	0.492	0.021
OK-1-130	3.904	24.666	0.236	1.133	0.028
OK-1-131	1.075	26.869	0.053	0.444	0.039
OK-1-132	3.217	38.753	0.193	3.015	0.034
OK-1-133	3.725	27.520	0.219	1.201	0.028
OK-1-134	0.717	24.845	0.045	0.251	0.043
OK-1-135	1.173	42.680	0.075	-0.263	0.042
OK-1-136	0.780	42.050	0.044	-0.139	0.044
OK-1-137	0.703	42.348	0.029	0.115	0.025
OK-1-138	0.774	36.517	0.043	0.194	0.033
OK-1-139	0.940	40.264	0.055	0.904	0.025
OK-1-140	0.836	29.752	0.046	0.056	0.023
OK-1-141	0.672	35.172	0.030	-0.077	0.037

OK-1-142	3.231	41.755	0.198	1.353	0.032
OK-1-143	2.779	27.581	0.152	0.734	0.030
OK-1-144	3.394	24.278	0.205	1.553	0.029
OK-1-145	3.290	26.902	0.201	0.921	0.027
OK-1-146	0.528	26.079	0.020	-0.300	0.037
OK-1-147	0.499	41.603	0.017	-0.004	0.034
OK-1-148	0.785	41.838	0.045	0.356	0.039
OK-1-149	3.662	41.201	0.226	0.648	0.027
OK-1-150	3.285	24.998	0.201	0.783	0.030
OK-1-151	2.457	28.610	0.118	1.458	0.037
OK-1-152	3.211	19.214	0.186	0.616	0.026
OK-1-153	2.666	27.545	0.156	1.747	0.033
OK-1-154	0.718	25.189	0.024	0.106	0.032
OK-1-155	3.370	39.629	0.219	1.470	0.028
OK-1-156	3.780	25.839	0.241	1.630	0.027
OK-1-157	0.432	27.929	0.026	-0.268	0.037
OK-1-158	0.545	42.267	0.033	-0.224	0.030
OK-1-159	2.748	40.134	0.178	1.921	0.042
OK-1-160	0.512	26.787	0.031	-0.395	0.039
OK-1-161	2.700	28.974	0.158	0.510	0.035
OK-1-162	0.316	43.698	0.027	-0.466	0.437
OK-1-163	1.970	37.697	0.089	2.772	0.098
OK-1-164	0.909	42.178	0.069	2.286	0.034
OK-1-165	0.349	43.614	0.032	-0.470	0.025
OK-1-166	0.382	37.708	0.015	0.352	0.053
OK-1-167	0.663	45.693	0.067	-0.366	0.034
OK-1-168	0.621	43.144	0.046	-0.293	0.042
OK-1-169	0.401	44.807	0.034	-0.413	0.069
OK-1-170	0.597	43.738	0.044	0.825	0.038
OK-1-171	1.093	44.290	0.061	0.018	0.052

OK-1-172	0.477	40.934	0.018	0.294	0.041
OK-1-173	0.974	39.069	0.065	0.013	0.066
OK-1-174	0.846	41.145	0.041	0.183	0.079
OK-1-175	2.239	34.958	0.034	-0.003	0.047
OK-1-176	0.551	37.650	0.033	0.074	0.055
OK-1-177	0.771	42.615	0.054	-0.080	1.231
OK-1-178	2.124	33.088	0.058	1.787	0.057
OK-1-179	0.431	42.093	0.031	0.479	0.064
OK-1-180	2.724	35.330	0.175	0.724	0.049
OK-1-181	0.702	43.047	0.034	-0.169	0.072
OK-1-182	0.387	44.194	0.023	0.034	0.041
OK-1-183	0.218	44.357	0.017	-0.380	0.031
OK-1-184	3.398	24.750	0.242	1.282	0.035
OK-1-185	0.744	42.841	0.055	-0.197	0.045
OK-1-186	1.079	34.356	0.074	0.272	0.049
OK-1-187	2.339	30.260	0.152	0.337	0.073
OK-1-188	3.039	36.951	0.166	0.746	0.033
OK-1-189	0.283	41.178	0.025	-0.206	0.049
OK-1-190	3.464	22.416	0.205	1.034	0.045
OK-1-191	0.269	43.050	0.013	-0.343	0.031
OK-1-192	0.288	41.081	0.017	-0.402	0.065
OK-1-193	4.090	29.986	0.205	0.954	0.020
OK-1-194	0.158	38.569	0.012	-0.222	0.036
OK-1-195	3.152	34.780	0.159	0.617	0.027
OK-1-196	1.343	37.525	0.074	0.163	0.057
OK-1-197	1.839	29.432	0.100	0.533	0.024
OK-1-198	3.013	25.748	0.192	1.120	0.022
OK-1-199	0.394	39.974	0.016	-0.220	0.023
OK-1-200	2.171	30.080	0.133	0.617	0.032
OK-1-201	0.737	43.182	0.042	-0.216	0.034

OK-1-202	0.170	43.835	0.014	-0.372	0.036
OK-1-203	0.706	42.292	0.036	-0.184	0.029
OK-1-204	2.964	34.923	0.159	0.868	0.045
OK-1-205	1.089	42.901	0.067	0.224	0.032
OK-1-206	0.668	41.785	0.027	-0.233	0.030
OK-1-207	0.926	43.537	0.072	-0.228	0.038
OK-1-208	2.342	39.940	0.132	0.676	0.036
OK-1-209	2.452	28.948	0.150	1.090	0.025
OK-1-210	3.386	26.171	0.216	1.943	0.034
OK-1-211	3.034	27.017	0.174	1.016	0.029
OK-1-212	0.849	43.369	0.038	-0.029	0.039
OK-1-213	3.340	25.769	0.242	2.133	0.052
OK-1-214	0.998	42.204	0.069	1.290	0.055
OK-1-215	3.651	24.011	0.253	2.714	0.049
OK-1-216	0.568	41.314	0.024	0.324	0.032
OK-1-217	0.557	3.316	0.064	0.529	-0.005
OK-1-218	0.291	43.521	0.019	-0.033	0.040
OK-1-219	4.731	22.003	0.312	1.661	0.045
OK-1-220	3.655	24.498	0.240	1.511	0.047
OK-1-221	4.097	19.129	0.298	3.553	0.067
OK-1-222	0.438	39.408	0.016	0.237	0.036
OK-1-223	3.128	24.943	0.242	1.785	0.039
OK-1-224	0.655	37.816	0.034	1.087	0.066
OK-1-225	3.405	24.141	0.220	1.673	0.039
OK-1-226	0.702	40.440	0.039	0.099	0.032
OK-1-227	1.537	42.434	0.085	2.196	0.109
OK-1-228	0.415	43.783	0.023	0.382	0.046
OK-1-229	3.741	19.656	0.261	1.700	0.042
OK-1-230	0.415	42.814	0.015	-0.068	0.035
OK-1-231	0.220	40.698	0.009	0.027	0.028

OK-1-232	0.357	42.838	0.028	-0.136	0.033
OK-1-233	0.722	42.759	0.038	-0.290	0.030
OK-1-234	0.813	42.672	0.041	0.240	0.032
OK-1-235	0.471	42.810	0.019	0.122	0.035
OK-1-236	0.833	42.935	0.039	0.056	0.034
OK-1-237	0.637	41.877	0.029	0.009	0.029
OK-1-238	-0.219	38.864	0.026	0.664	3.981
OK-1-239	1.723	39.855	0.097	1.026	0.035
OK-1-240	3.169	31.146	0.161	2.171	0.028

Normalized Minor/Trace Element Concentrations for I-35 Outcrop (ppm)					
Sample	Ni	Cu	Mo	Ba	Zr
OK-1-1	43.099	6.513	73.914	1353.144	93.515
OK-1-2	97.406	41.676	64.454	374.277	63.111
OK-1-3	59.436	12.334	64.456	1683.245	88.634
OK-1-4	28.095	4.046	15.792	585.597	36.545
OK-1-5	42.253	2.067	67.863	1108.272	70.227
OK-1-6	11.647	3.387	18.869	273.954	37.140
OK-1-7	128.273	64.222	168.908	2059.015	76.494
OK-1-8	23.612	6.340	16.673	235.142	35.655
OK-1-9	79.973	30.730	152.258	2548.524	74.721
OK-1-10	76.681	24.573	117.686	1915.420	90.095
OK-1-11	86.530	24.912	162.234	2227.283	78.342
OK-1-12	73.958	8.483	114.352	3575.344	72.557
OK-1-13	124.915	23.264	795.195	5400.484	57.591
OK-1-14	96.859	9.296	114.962	655.047	73.269
OK-1-15	99.667	11.162	131.059	695.005	91.870
OK-1-16	80.293	14.132	97.877	704.102	72.254
OK-1-17	80.213	11.328	122.858	402.817	79.432
OK-1-18	35.360	6.413	31.509	458.397	36.431

OK-1-19	26.217	10.072	28.672	481.932	38.991
OK-1-20	61.281	16.341	54.137	350.410	57.651
OK-1-21	101.367	11.728	102.184	1236.189	82.908
OK-1-22	97.677	33.596	110.016	314.234	82.890
OK-1-23	118.521	10.331	130.568	473.260	78.949
OK-1-24	43.081	35.160	118.539	195.400	54.268
OK-1-25	75.286	11.099	157.135	362.420	69.764
OK-1-26	35.501	6.749	36.229	691.360	38.168
OK-1-27	78.065	6.154	137.218	739.267	73.339
OK-1-28	92.417	21.225	194.361	717.285	71.219
OK-1-29	0.000	1.795	5.565	570.538	32.512
OK-1-30	104.133	14.954	188.663	700.285	75.956
OK-1-31	89.554	12.813	170.180	337.695	72.960
OK-1-32	78.349	7.466	103.951	796.507	53.775
OK-1-33	92.191	15.772	182.143	1079.243	81.982
OK-1-34	22.283	1.780	28.629	498.589	35.784
OK-1-35	65.927	25.200	94.285	1578.477	62.262
OK-1-36	27.271	5.507	22.895	490.549	39.326
OK-1-37	10.900	14.145	97.664	672.075	48.516
OK-1-38	20.170	0.000	22.594	254.949	33.597
OK-1-39	28.770	5.445	67.578	621.178	42.711
OK-1-40	83.926	16.822	111.621	531.333	69.864
OK-1-41	73.686	34.834	68.141	454.427	39.103
OK-1-42	84.861	21.167	110.675	1428.372	78.772
OK-1-43	97.548	15.773	126.663	1067.079	88.710
OK-1-44	7.672	4.916	22.272	664.141	37.905
OK-1-45	0.000	5.015	32.809	614.642	40.619
OK-1-46	0.000	3.367	1.734	689.863	38.048
OK-1-47	2.420	0.000	10.299	845.730	35.342
OK-1-48	64.298	5.746	102.852	912.646	75.506

OK-1-49	90.810	8.442	108.223	502.605	76.445
OK-1-50	24.601	11.864	13.648	828.670	39.425
OK-1-51	76.594	34.128	57.760	1109.519	72.960
OK-1-52	0.000	2.738	36.552	548.603	34.309
OK-1-53	14.706	26.069	43.689	593.926	43.874
OK-1-54	73.717	7.068	156.286	614.892	73.978
OK-1-55	41.370	12.778	36.103	646.864	43.069
OK-1-56	103.506	14.726	159.709	1343.928	70.191
OK-1-57	44.117	10.440	56.707	686.637	49.564
OK-1-58	29.055	8.944	32.642	1008.899	37.234
OK-1-59	87.639	8.160	175.098	861.701	75.739
OK-1-60	74.948	15.918	189.437	1366.504	83.000
OK-1-61	31.850	4.922	26.460	681.786	43.454
OK-1-62	35.203	9.429	52.171	954.754	38.705
OK-1-63	75.395	18.392	93.644	2444.054	69.132
OK-1-64	24.012	12.606	37.154	580.581	40.491
OK-1-65	25.881	3.773	57.068	546.851	38.236
OK-1-66	86.969	77.673	217.566	574.652	72.400
OK-1-67	52.659	22.033	21.929	454.867	36.105
OK-1-68	131.910	76.882	33.454	1759.345	32.875
OK-1-69	17.981	12.997	0.039	421.164	34.159
OK-1-70	56.000	15.462	68.489	886.199	74.733
OK-1-71	49.073	11.522	71.133	570.225	60.906
OK-1-72	32.524	17.035	58.032	924.778	47.032
OK-1-73	39.635	29.422	24.761	540.703	40.511
OK-1-74	156.217	99.382	203.699	2024.611	63.282
OK-1-75	52.444	30.847	44.488	565.882	40.613
OK-1-76	95.795	49.142	179.774	346.295	73.505
OK-1-77	28.061	27.025	32.546	621.486	40.390
OK-1-78	79.113	17.107	186.402	1247.267	70.821

OK-1-79	57.921	7.260	150.838	1469.867	65.889
OK-1-80	32.118	12.796	30.766	777.249	44.876
OK-1-81	39.770	12.560	31.457	668.936	35.968
OK-1-82	20.623	9.981	23.775	544.377	37.708
OK-1-83	26.339	23.644	25.257	400.755	39.832
OK-1-84	69.990	5.377	184.442	464.553	61.130
OK-1-85	18.792	10.010	53.171	361.927	37.509
OK-1-86	33.054	6.989	32.269	296.500	33.644
OK-1-87	64.561	6.012	181.787	341.226	63.395
OK-1-88	42.417	13.033	57.322	782.588	38.556
OK-1-89	48.179	12.748	64.906	819.612	38.223
OK-1-90	66.216	6.830	164.594	554.740	65.304
OK-1-91	53.775	15.311	31.313	413.776	38.968
OK-1-92	68.865	19.782	26.409	401.690	39.936
OK-1-93	58.592	18.581	49.260	489.427	38.971
OK-1-94	29.276	3.821	35.954	293.793	39.714
OK-1-95	65.957	8.397	160.286	360.064	71.991
OK-1-96	25.930	10.920	41.330	603.618	37.143
OK-1-97	68.683	14.380	125.210	567.588	71.215
OK-1-98	27.168	7.336	19.836	388.549	35.026
OK-1-99	43.888	11.064	58.877	772.723	35.909
OK-1-100	80.846	16.035	237.990	958.529	71.091
OK-1-101	346.790	203.247	134.340	1219.930	66.607
OK-1-102	71.795	29.717	43.709	2237.387	4.393
OK-1-103	71.688	21.185	108.695	923.676	76.046
OK-1-104	63.663	9.922	178.547	770.536	82.030
OK-1-105	300.737	164.648	146.643	802.814	52.094
OK-1-106	38.342	8.263	44.302	886.233	51.960
OK-1-107	23.285	12.354	46.597	1118.712	34.839
OK-1-108	71.221	31.474	164.430	557.717	81.625

OK-1-109	13.940	9.359	16.438	2337.424	29.892
OK-1-110	73.189	45.256	95.164	610.078	84.512
OK-1-111	79.441	26.893	55.530	1595.145	80.289
OK-1-112	23.909	30.134	34.578	1808.599	35.444
OK-1-113	75.359	24.707	192.921	727.188	70.934
OK-1-114	48.968	28.756	49.314	705.062	34.542
OK-1-115	88.819	54.249	151.555	435.407	76.842
OK-1-116	79.954	27.426	161.757	605.514	82.879
OK-1-117	67.463	25.828	98.688	419.678	72.543
OK-1-118	71.531	59.145	141.009	503.250	74.759
OK-1-119	37.272	48.040	68.568	683.811	38.555
OK-1-120	42.166	45.925	117.871	745.120	36.956
OK-1-121	76.552	44.852	145.389	864.629	79.326
OK-1-122	78.565	34.570	164.889	264.704	80.792
OK-1-123	129.326	65.228	207.894	377.313	72.494
OK-1-124	61.911	34.417	49.499	655.045	59.794
OK-1-125	133.371	80.222	238.548	447.906	74.237
OK-1-126	89.739	68.861	113.762	412.633	67.913
OK-1-127	58.678	30.726	60.382	1185.796	36.561
OK-1-128	71.412	27.178	86.386	1225.048	35.558
OK-1-129	94.528	40.071	149.927	942.127	73.328
OK-1-130	99.540	20.233	260.570	648.257	75.768
OK-1-131	54.078	29.056	65.562	940.942	36.531
OK-1-132	122.850	75.162	343.382	853.267	64.814
OK-1-133	94.161	26.508	284.227	596.488	79.170
OK-1-134	45.767	37.066	86.717	967.530	37.086
OK-1-135	31.087	6.266	79.534	851.490	45.743
OK-1-136	22.591	7.939	79.294	1050.715	37.481
OK-1-137	59.767	18.432	84.706	1011.725	35.451
OK-1-138	19.470	7.603	37.406	820.064	34.247

OK-1-139	29.855	1.465	117.682	492.501	46.655
OK-1-140	20.109	7.613	66.960	941.097	38.102
OK-1-141	67.675	25.736	82.837	634.269	35.077
OK-1-142	78.502	17.162	224.549	432.209	67.158
OK-1-143	79.064	36.141	234.671	26.842	64.594
OK-1-144	76.991	37.538	222.840	425.942	68.771
OK-1-145	68.050	29.248	177.362	730.257	68.006
OK-1-146	3.239	0.000	46.893	668.886	29.019
OK-1-147	47.390	25.354	54.229	588.329	32.147
OK-1-148	109.168	47.064	55.601	1332.527	33.094
OK-1-149	76.301	22.459	222.757	0.000	78.154
OK-1-150	74.509	11.933	182.747	349.255	66.819
OK-1-151	280.875	158.254	175.791	1648.199	33.976
OK-1-152	54.371	12.936	128.439	991.313	60.483
OK-1-153	304.850	252.891	348.043	1302.652	51.793
OK-1-154	21.010	46.360	42.056	622.036	31.609
OK-1-155	65.161	25.167	181.746	831.456	61.453
OK-1-156	47.804	26.757	133.817	772.618	78.925
OK-1-157	13.783	6.762	76.241	480.439	36.066
OK-1-158	14.395	3.761	51.589	670.971	36.036
OK-1-159	80.735	73.064	173.848	2088.011	58.931
OK-1-160	3.148	4.646	17.095	294.729	35.522
OK-1-161	58.276	19.021	112.660	532.676	59.816
OK-1-162	31.490	67.644	69.351	299.274	34.267
OK-1-163	13.372	40.047	184.241	700.796	36.099
OK-1-164	15.647	44.133	234.148	762.117	38.883
OK-1-165	1.966	4.004	13.452	555.676	35.429
OK-1-166	0.000	22.456	35.522	607.877	34.914
OK-1-167	29.096	13.147	79.128	470.578	39.721
OK-1-168	9.667	4.050	51.125	521.719	36.405

OK-1-169	34.717	212.308	54.563	655.752	35.795
OK-1-170	0.000	19.024	18.633	472.048	35.576
OK-1-171	62.811	53.922	4.882	526.185	38.078
OK-1-172	14.065	24.548	19.180	582.384	32.906
OK-1-173	17.843	23.435	28.154	357.150	39.759
OK-1-174	28.106	22.038	19.773	269.746	39.808
OK-1-175	37.160	31.653	10.918	559.629	34.166
OK-1-176	6.705	12.423	9.011	347.250	34.218
OK-1-177	5.716	9.302	13.835	772.871	38.348
OK-1-178	7.673	32.696	22.686	878.414	36.981
OK-1-179	0.000	5.871	25.498	422.576	32.248
OK-1-180	48.097	46.657	28.595	194.540	51.121
OK-1-181	8.511	18.434	4.687	330.980	34.992
OK-1-182	4.898	7.927	0.912	192.283	32.181
OK-1-183	13.542	18.652	0.000	542.449	32.433
OK-1-184	193.241	116.209	0.000	396.648	78.371
OK-1-185	36.369	56.115	5.314	619.957	39.070
OK-1-186	53.701	16.163	18.464	762.631	20.064
OK-1-187	130.900	158.962	0.000	368.267	62.342
OK-1-188	180.863	422.737	43.577	664.898	63.497
OK-1-189	2.420	18.607	16.861	453.930	33.006
OK-1-190	225.129	521.526	46.926	823.074	61.876
OK-1-191	20.850	44.459	4.018	406.163	32.233
OK-1-192	18.426	62.187	32.814	473.632	33.134
OK-1-193	140.540	533.515	188.055	1707.055	57.200
OK-1-194	0.000	13.900	14.540	264.978	33.285
OK-1-195	85.468	20.813	81.280	986.680	63.922
OK-1-196	31.676	22.725	46.875	593.968	41.917
OK-1-197	80.501	72.304	10.867	318.929	54.368
OK-1-198	112.365	26.527	9.980	636.009	65.170

OK-1-199	16.283	9.532	8.325	280.969	33.245
OK-1-200	62.708	11.025	5.655	677.972	54.326
OK-1-201	39.939	39.181	3.773	771.307	37.683
OK-1-202	26.038	23.051	5.020	248.490	33.826
OK-1-203	15.631	13.324	9.462	237.441	34.552
OK-1-204	148.162	76.336	20.228	1810.864	52.315
OK-1-205	36.885	27.910	10.875	1010.236	40.061
OK-1-206	14.042	28.215	1.560	522.024	34.089
OK-1-207	20.027	17.090	4.364	622.501	41.613
OK-1-208	93.766	97.593	7.709	894.798	53.671
OK-1-209	184.512	111.104	8.587	757.792	63.075
OK-1-210	229.450	105.305	31.746	1145.556	64.946
OK-1-211	143.097	36.902	24.237	1296.724	63.468
OK-1-212	59.644	39.960	7.924	791.584	37.835
OK-1-213	163.756	58.768	609.974	416.739	74.748
OK-1-214	255.587	64.635	297.200	1378.945	42.076
OK-1-215	190.306	122.694	395.928	730.189	73.491
OK-1-216	23.297	17.250	25.281	848.159	33.837
OK-1-217	35.356	26.302	17.100	6094.356	0.000
OK-1-218	22.001	19.593	40.066	583.096	34.696
OK-1-219	192.037	71.749	120.897	1997.446	82.727
OK-1-220	168.320	53.821	534.585	621.370	77.336
OK-1-221	215.258	84.640	814.374	378.016	86.464
OK-1-222	111.051	23.460	163.306	789.429	35.471
OK-1-223	188.466	71.537	519.118	659.431	78.205
OK-1-224	33.782	13.343	220.589	822.655	35.590
OK-1-225	161.404	53.231	619.639	967.092	71.128
OK-1-226	93.031	87.934	205.293	802.701	36.641
OK-1-227	80.682	21.313	419.518	624.479	41.695
OK-1-228	143.596	31.653	265.232	680.084	35.730

OK-1-229	233.717	82.383	813.665	779.861	74.078
OK-1-230	89.164	27.391	175.915	751.017	36.672
OK-1-231	83.766	18.207	160.148	374.722	36.637
OK-1-232	48.906	24.922	82.640	725.906	34.721
OK-1-233	18.440	6.072	11.736	1299.358	39.925
OK-1-234	65.679	37.636	8.823	1445.345	37.686
OK-1-235	35.887	24.625	3.683	1532.279	34.326
OK-1-236	40.228	41.358	1.475	1686.569	38.122
OK-1-237	21.591	22.855	6.146	1221.673	36.298
OK-1-238	32.521	22.503	8.337	1029.490	22.783
OK-1-239	113.714	95.870	10.580	1989.799	43.643
OK-1-240	138.547	283.611	13.194	2723.680	58.907

RTC-WS-220 Standard Major Element Concentrations (wt%)					
	Al	Si	Ti	Fe	P
STND 1	5.6279074	33.9272137	0.11396551	0.26587006	2.5658189
STND 2	5.43456444	32.8940955	0.09220949	0.26119336	2.6109914
STND 3	5.2513414	31.7527334	0.08136506	0.25807799	2.6054643
STND 4	5.42716982	32.7997773	0.08196656	0.2687182	2.6540974
STND 5	5.60450154	34.1474966	0.11472283	0.2713651	2.7255377
STND 6	5.6643727	34.3527816	0.1143208	0.26505944	2.5976533
STND 7	5.45058798	33.2511707	0.08102566	0.26317172	2.6264404
STND 8	5.59411372	34.1122019	0.10636985	0.26491814	2.6241562
STND 9	5.63018247	34.2843949	0.09612992	0.28202126	2.7631329
STND 10	5.5769737	33.9046174	0.1150581	0.27406151	2.6977518
STND 11	5.46975626	32.940423	0.09494552	0.27688401	2.7800688
STND 12	5.61898949	33.9345084	0.10651492	0.275417	2.7092465
STND 13	5.63250618	33.979746	0.10898897	0.28333692	2.7445552
STND 14	5.62379698	33.9601137	0.1144617	0.27128074	2.7501601
STND 15	5.37787288	32.4859825	0.09149124	0.28731427	2.7595345

STND 16	5.67171745	34.2378879	0.11702812	0.27739036	2.6153119
STND 17	5.68567804	34.2100812	0.11236774	0.27753507	2.681308
STND 18	5.48955261	33.4435993	0.09306854	0.28189639	2.7500046
STND 19	5.54402023	33.9501317	0.09629618	0.28180128	2.7507258
STND 20	5.4076582	32.6380915	0.08916292	0.27775469	2.8060052
STND 21	5.36288433	32.7480025	0.08898531	0.2786833	2.7855468
STND 22	5.48773104	32.8781615	0.09847888	0.28562758	2.822094
STND 23	5.54450231	33.6122574	0.10750348	0.28089832	2.8705598
STND 24	5.54077448	33.871783	0.11568956	0.27941051	2.8199555
STND 25	5.53692697	33.6093514	0.09741218	0.2806535	2.8411207
STND 26	5.52819175	33.9164393	0.11565951	0.27624594	2.8784455
STND 27	5.55196234	33.8717543	0.103622	0.27816164	2.8602792
STND 28	5.62065391	34.057715	0.11174366	0.28143515	2.853365
STND 29	5.6170823	34.0945369	0.10753418	0.28807123	2.8859539
STND 30	5.48448338	33.8580992	0.11130742	0.28011114	2.8285949
STND 31	5.63468764	34.0340303	0.10679915	0.2708198	2.7433316
STND 32	5.58742565	34.2832356	0.10856769	0.27868607	2.8261409
STND 33	5.62698352	34.0952734	0.10955229	0.28535816	2.8709071
STND 34	5.55489954	33.7399885	0.10789766	0.28540917	2.8858978
STND 35	5.39566703	32.8929443	0.09070171	0.28159137	2.8860422
STND 36	5.56753401	34.048998	0.10899534	0.2871745	2.8307035
STND 37	5.40629204	32.9599933	0.09631123	0.26944896	2.8509001
STND 38	5.58059344	34.2196219	0.1135457	0.28522452	2.8531435
STND 39	5.53644741	33.8983761	0.10174187	0.2799252	2.8783786
STND 40	5.53152205	34.2028508	0.11731018	0.27908264	2.8798466
STND 41	5.54816111	34.3124916	0.11558032	0.27899333	2.8469596
STND 42	5.53065451	34.3583753	0.10861548	0.28689348	2.8548047
STND 43	5.50258108	34.2526121	0.11381257	0.291603	2.8225121
STND 44	5.38399427	34.3524723	0.12027717	0.28088466	2.8649266
STND 45	5.29677563	32.8706236	0.09521998	0.27806696	2.830737

STND 46	5.51808785	34.2729132	0.11575323	0.2702078	2.8318848
STND 47	5.47648565	34.1731278	0.10870365	0.28222194	2.7982887
STND 48	5.51345897	34.325127	0.10109238	0.275254	2.8333016
STND 49	5.52996499	34.3322231	0.10916579	0.27332238	2.8559841
STND 50	5.44954193	34.3903386	0.10346266	0.28116026	2.835253
STND 51	5.508018	34.4069857	0.11619584	0.2881001	2.8736595
STND 52	5.28293103	33.1112898	0.096364	0.27968578	2.8774098
STND 53	5.37551604	33.464597	0.09268341	0.27826028	2.853713
STND 54	5.27816601	33.1323219	0.08908006	0.27526599	2.8954217
STND 55	5.49791235	33.82071	0.11044865	0.27870638	2.8212309
STND 56	5.54083403	34.305115	0.12175496	0.28039851	2.8095497
STND 57	5.41808694	33.1392554	0.09036178	0.27959864	2.861751
STND 58	5.55660024	34.3911214	0.12012452	0.28399812	2.8269663
STND 59	5.3687727	32.956871	0.09977034	0.27323	2.8388574
STND 60	5.5671494	34.110496	0.10175781	0.27035598	2.8561062
STND 61	5.46518068	33.9755769	0.11498842	0.28613421	2.824703
STND 62	5.26000917	32.7107863	0.09202521	0.26852067	2.8317163
STND 63	5.43222925	34.1223827	0.10520299	0.28484671	2.8318664
STND 64	5.45453219	34.3192949	0.11582258	0.28157761	2.8488509
STND 65	5.40487863	33.9794887	0.10970892	0.284916	2.8358303
STND 66	5.32746267	33.1917047	0.08660689	0.26936261	2.8220365
STND 67	5.47319733	34.1916603	0.10965505	0.27787695	2.8559099
STND 68	5.41987036	34.1367042	0.11390316	0.28224457	2.8916829
STND 69	5.31790738	33.3463408	0.10228709	0.27846878	2.8323985
STND 70	5.26245719	32.8851334	0.08900672	0.28038796	2.8750167
STND 71	5.50027941	34.2418355	0.11197846	0.27712581	2.8426271
STND 72	5.33700483	33.1898386	0.09768584	0.27883503	2.8671268
STND 73	5.37827199	34.1737544	0.12208724	0.27836862	2.8607993
STND 74	5.33692879	33.3364881	0.0855499	0.27376759	2.9287265
STND 75	5.44777498	34.2802176	0.1118447	0.28657167	2.8479086

STND 76	5.60422994	34.1362426	0.10547787	0.27858414	2.8242827
STND 77	5.32025982	32.9965688	0.09031411	0.27210272	2.8555158
STND 78	5.3271694	33.2724396	0.11343629	0.27063072	2.8562306
STND 79	5.53732728	34.4405572	0.10810818	0.28067924	2.8162213
STND 80	5.35512518	32.9951752	0.08712322	0.26849231	2.864237
STND 81	5.53816544	33.9109568	0.11666943	0.27072437	2.8372981
STND 82	5.46706848	33.4469763	0.09899793	0.28112358	2.8572812
STND 83	5.44667131	33.4366438	0.10832782	0.27786988	2.8480125
STND 84	5.25990572	32.1652937	0.0995113	0.2704761	2.8445812
STND 85	5.36901085	32.8031224	0.10961835	0.27685257	2.8108695
STND 86	5.25445453	32.1083086	0.09765857	0.27221266	2.8783337
STND 87	5.39310161	33.3494652	0.10608392	0.27742082	2.9344818
STND 88	5.28851013	32.9751368	0.15009581	0.27605992	2.9456988
STND 89	5.14471794	31.8290897	0.13682032	0.27192977	2.9694006
STND 90	4.86698823	30.4211934	0.12504803	0.26771725	2.9491594
STND 91	5.34680662	32.6885746	0.09976117	0.26815069	2.834926
STND 92	5.14323148	31.69559	0.10326266	0.2847294	2.8764044
STND 93	5.45808772	32.8094895	0.0917069	0.27234837	2.8066901
STND 94	5.46275106	33.4768194	0.09747428	0.27442699	2.7456229
STND 95	5.50393204	32.8799992	0.10021557	0.27391147	2.7838813
STND 96	5.46070466	33.011157	0.08542275	0.27309685	2.7350531
STND 97	5.49155202	33.2107066	0.1037958	0.27045336	2.7565947
STND 98	5.46501524	33.020879	0.09950466	0.27366966	2.7641403
STND 99	5.49889238	33.3822378	0.10720239	0.27201694	2.7817535
STND 100	5.5512327	33.4541549	0.1054267	0.27510019	2.7787231
STND 101	5.27247123	31.7053289	0.08189318	0.26748611	2.7252038
STND 102	5.26997879	31.8920927	0.07759304	0.2650313	2.7303119
STND 103	5.3046053	32.1298371	0.07798605	0.27723532	2.706368
STND 104	5.32943204	32.7532122	0.10218977	0.26170906	2.8184423
STND 105	5.37397016	32.986329	0.10531477	0.26436165	2.7790926

STND 106	5.49030656	33.8580681	0.10131814	0.27266802	2.7851062
STND 107	5.60133637	33.7737135	0.11605429	0.27768646	2.7953222
STND 108	5.54229363	33.8102238	0.119587	0.27319491	2.8279667
STND 109	5.59852184	33.8968886	0.1202398	0.26820401	2.7872508
STND 110	5.58353576	33.7182816	0.10109908	0.27273186	2.8117064
STND 111	5.48194024	33.0740935	0.11225596	0.2710386	2.824726
STND 112	5.51520076	33.2987241	0.10529653	0.27415538	2.7943346
STND 113	5.36162669	32.4055215	0.09805812	0.2700843	2.795297
STND 114	5.2899916	32.2166343	0.1034218	0.27187397	2.7747682
STND 115	5.32732903	32.1342923	0.09263262	0.26907046	2.7763939
STND 116	5.3153174	31.8919791	0.09580566	0.27027657	2.8318281
STND 117	5.23241212	31.8058535	0.07970045	0.26412923	2.7694447
STND 118	5.06629004	30.9483651	0.09011252	0.26698849	2.7782346
STND 119	5.28641117	31.6595144	0.08959144	0.2681685	2.7813691
STND 120	5.27519171	32.0299323	0.09811124	0.27246454	2.7671346
Ave (wt%)	5.4459605	33.3880533	0.10378935	0.27584698	2.8089282
STD Dev	0.13716434	0.84610779	0.01216262	0.0067016	0.0748268

RTC-WS-220 Standard Minor/Trace Element Concentrations (ppm)						
	Ni	Cu	Mo	Ba	Co	Zr
STND 1	133.6054	103.7677	67.90784	1639.812	16.20668	110.7396
STND 2	133.8177	108.53	76.0706	1920.078	16.45378	111.2168
STND 3	128.8908	109.5712	75.55428	2323.06	16.45145	110.687
STND 4	126.8589	107.6717	74.64342	1753.934	15.36748	111.1351
STND 5	134.8778	106.79	77.67354	1600.862	14.87043	112.6828
STND 6	133.5388	114.4734	71.27863	2526.992	16.96757	110.2965
STND 7	138.1126	107.8867	74.03935	1919.091	15.5191	110.8515
STND 8	138.3901	107.053	70.99504	1684.19	14.82535	110.22
STND 9	134.9464	107.1873	72.45111	1927.389	15.17037	112.2066
STND 10	140.6511	114.5596	72.68035	2486.404	16.01019	112.1479

STND 11	136.5087	107.3012	74.0204	1204.931	15.5378	110.067
STND 12	133.1984	108.0288	73.01894	2480.685	13.92687	111.0405
STND 13	141.176	109.4928	74.96777	2272.204	15.67136	112.9345
STND 14	128.9768	110.0802	68.40911	2436.006	16.99855	109.863
STND 15	136.8575	114.6306	78.10209	2549.116	14.67709	110.7634
STND 16	134.2873	110.1645	74.75369	2702.162	15.75041	112.1323
STND 17	133.1451	114.6968	76.07135	2623.148	15.65103	110.4036
STND 18	137.0732	113.7578	75.97649	2445.477	17.54929	112.4382
STND 19	137.0384	106.575	68.30799	1538.366	17.14576	106.6549
STND 20	131.0811	106.2637	72.3617	1559.588	17.53092	111.3438
STND 21	128.8327	111.0496	74.54829	2647.109	15.73119	111.7878
STND 22	135.6688	107.5993	72.17652	1812.67	16.53075	109.0278
STND 23	137.2346	111.8237	75.41201	1644.746	16.68505	110.728
STND 24	131.5725	110.4891	78.85803	2629.048	15.70897	110.4717
STND 25	140.4695	112.8689	70.27077	1094.927	15.19555	111.5221
STND 26	137.0221	110.398	77.31109	1698.997	16.64021	111.0264
STND 27	134.2859	105.7544	72.17713	2330.245	13.29536	110.1638
STND 28	132.596	105.2864	72.81748	2064.345	17.63259	110.09
STND 29	139.1219	111.5169	71.73916	1830.673	14.0397	108.3603
STND 30	133.2639	109.2969	75.76267	2365.269	14.99257	109.2305
STND 31	131.0576	104.5967	70.35892	1963.124	16.06061	109.387
STND 32	134.4304	108.1244	77.83213	2484.982	15.80158	112.2457
STND 33	131.7489	112.5727	74.84626	1652.738	16.24927	111.9763
STND 34	136.7215	117.3009	73.12311	1791.906	16.95353	113.2182
STND 35	127.8265	111.2332	74.34111	1752.731	14.51992	109.115
STND 36	133.4893	110.807	73.97068	2363.174	13.08252	109.2073
STND 37	139.1641	112.122	79.01902	2419.773	16.80658	108.3135
STND 38	134.8732	106.4481	73.7889	1081.27	15.89045	111.9549
STND 39	132.5676	102.9471	74.7466	2036.176	15.72143	111.6446
STND 40	135.0342	107.9232	71.89422	2774.271	16.50999	111.4665

STND 41	135.1464	106.0251	74.43924	1772.076	15.80955	111.884
STND 42	140.6159	114.9194	71.1314	1433.556	15.66212	111.189
STND 43	135.0012	111.7143	68.34951	1421.406	16.32162	110.2733
STND 44	135.7146	114.3427	72.31341	1413.401	14.88012	111.686
STND 45	135.6705	110.4033	71.66291	1924.205	13.77593	110.7247
STND 46	135.9132	111.8723	71.72948	1454.563	15.10198	110.6529
STND 47	141.2189	115.423	73.8224	2222.528	17.4224	111.5726
STND 48	136.2503	112.1376	72.8318	1425.508	14.45034	110.9815
STND 49	130.5067	111.7309	76.7006	2728.557	14.85062	109.6553
STND 50	136.2023	113.1339	74.49966	2833.687	16.6269	109.9681
STND 51	136.9678	111.0137	75.63894	2456.885	16.03047	112.8701
STND 52	138.3809	111.4311	76.17829	2292.406	16.81122	110.692
STND 53	129.3379	105.426	73.68903	1922.36	14.75965	110.5795
STND 54	141.2661	110.679	72.95886	1598.627	13.56779	111.141
STND 55	134.9918	112.5414	70.95083	2221.209	16.47844	111.9822
STND 56	137.6433	107.2331	68.42759	2154.144	14.19191	111.3218
STND 57	136.0811	113.1439	74.34606	2566.899	15.05083	113.5293
STND 58	132.4858	107.5297	75.52511	2127.887	15.81596	111.4836
STND 59	133.9647	108.6599	71.7897	850.2728	14.33607	110.5611
STND 60	135.6939	110.2317	75.32194	2802.193	15.87779	111.2526
STND 61	135.2305	110.8072	78.10264	2393.49	16.92999	108.9535
STND 62	134.4198	107.6544	73.1193	1794.671	14.46696	109.2393
STND 63	131.6718	108.7591	69.05695	2195.112	14.51329	110.3294
STND 64	138.0795	107.4486	73.70546	1848.142	16.33207	111.7723
STND 65	128.1295	111.251	73.85877	2344.896	16.4512	110.5335
STND 66	133.2297	106.0793	74.52033	1865.132	14.46716	109.7857
STND 67	133.5586	110.1078	71.70031	1866.73	16.00786	108.7336
STND 68	134.2596	115.0057	71.97575	2538.84	14.62974	112.2431
STND 69	138.8197	110.6712	73.89061	2184.573	15.385	111.1164
STND 70	133.89	112.5794	74.82423	1792.135	15.32121	111.4996

STND 71	131.9136	111.2547	76.68886	1760.32	14.12791	110.9373
STND 72	133.0787	109.6097	72.4933	2175.49	18.25238	111.4868
STND 73	135.0657	112.6491	72.34173	1849.299	16.52055	109.8711
STND 74	137.2882	109.3949	75.56777	3074.34	14.34009	113.4821
STND 75	130.2213	105.6871	75.94703	1997.354	15.04896	110.9322
STND 76	133.9515	109.209	70.8187	1568.661	15.17547	111.9779
STND 77	136.2731	111.8896	77.91221	2453.14	14.45669	114.0068
STND 78	129.757	106.9854	74.92327	1640.765	16.10176	111.1983
STND 79	136.3664	107.8209	69.76684	2524.974	12.30711	109.7538
STND 80	130.1123	112.4647	73.58182	2479.362	15.18093	110.1146
STND 81	135.3799	110.9971	72.81243	1969.657	15.20142	108.2365
STND 82	137.0685	112.6915	69.36332	1944.784	15.77123	112.889
STND 83	128.1212	111.0075	73.77185	1790.85	15.68665	109.5518
STND 84	138.9432	107.2151	70.77382	2404.052	14.92521	112.1944
STND 85	136.6359	111.2134	76.27478	2393.17	16.88428	111.1592
STND 86	127.8963	109.2737	75.8406	2019.394	18.49294	111.9071
STND 87	131.0834	109.7804	72.13052	2729.272	16.36356	107.4002
STND 88	137.1622	108.7134	77.25696	1411.601	16.54858	111.4557
STND 89	133.1716	108.1731	71.59891	1883.257	17.25428	109.7315
STND 90	137.5918	105.853	75.62762	2539.465	15.86886	110.2913
STND 91	134.9934	111.8903	73.59168	1815.223	16.52053	111.4845
STND 92	133.3331	110.9905	75.34106	1258.502	13.99841	110.7642
STND 93	133.8929	109.027	79.66975	1931.462	17.01487	114.2215
STND 94	131.2779	112.0057	77.70002	1115.531	15.28684	111.9771
STND 95	133.8816	108.1699	70.02735	1555.548	14.24626	113.8523
STND 96	135.3263	105.284	69.1163	3068.825	13.84963	111.4029
STND 97	134.9532	112.1845	74.58002	1906.341	15.883	110.5216
STND 98	133.2729	110.8435	73.72071	2081.328	13.91421	112.8929
STND 99	136.0844	113.5065	75.80216	2882.147	12.72427	112.478
STND 100	131.1856	100.5884	72.10753	2923.366	16.10152	111.6611

STND 101	130.0912	109.0312	74.97977	1353.781	17.37021	110.2803
STND 102	137.4184	111.9188	77.39865	1672.427	17.05132	112.2868
STND 103	131.8381	111.732	74.25366	2212.483	15.71787	111.1231
STND 104	132.215	108.9786	79.14137	2140.732	14.51607	110.6843
STND 105	137.4309	111.0502	71.2927	2483.793	15.50988	109.5686
STND 106	142.5158	110.9476	73.60997	1429.654	15.48348	112.3225
STND 107	135.5772	113.5379	78.65572	1070.069	17.65263	113.5022
STND 108	127.5954	104.5424	75.20654	2036.28	14.70956	111.0623
STND 109	136.1209	112.3902	77.79022	1653.773	14.09846	113.7578
STND 110	129.0895	108.5668	73.91862	2307.659	16.88268	112.1026
STND 111	131.8242	110.0497	76.0089	1304.118	16.18729	110.7579
STND 112	134.745	115.8313	73.7805	2712.769	17.14879	111.844
STND 113	132.266	109.2155	72.70778	2155.09	15.10028	110.777
STND 114	136.1708	112.0555	73.19082	1908.218	14.69057	110.9034
STND 115	133.335	109.2682	72.09202	2208.608	14.16777	109.0101
STND 116	138.7764	109.9108	73.63198	2885.222	17.66833	112.7543
STND 117	128.7175	112.6391	75.24653	1639.327	16.11182	109.1938
STND 118	137.3093	110.7642	70.63501	1348.117	14.02753	112.2182
STND 119	132.1855	112.8458	76.13804	1602.346	18.47476	109.6505
STND 120	138.1242	108.4965	67.61539	2050.057	15.4033	111.3313
Ave (wt%)	134.492	109.99	73.7982	2031.66	15.639	111.0328
STD Dev	3.35259	2.9362	2.65957	483.59	1.21898	1.37422

Appendix B - XRD Diffractograms

